Author/s:
Gruber, E;So, J;Lewis, AC;Franich, R;Cole, R;Martelotto, LG;Rogers, AJ;Vidacs, E;Fraser, P;Stanley, K;Jones, L;Trigos, A;Thio, N;Li, J;Nicolay, B;Daigle, S;Tron, AE;Hyer, ML;Shortt, J;Johnstone, RW;Kats, LM

Title:
Inhibition of mutant IDH1 promotes cycling of acute myeloid leukemia stem cells

Date:
2022-08-16

Citation:
Gruber, E., So, J., Lewis, A. C., Franich, R., Cole, R., Martelotto, L. G., Rogers, A. J., Vidacs, E., Fraser, P., Stanley, K., Jones, L., Trigos, A., Thio, N., Li, J., Nicolay, B., Daigle, S., Tron, A. E., Hyer, M. L., Shortt, J. ,... Kats, L. M. (2022). Inhibition of mutant IDH1 promotes cycling of acute myeloid leukemia stem cells. Cell Reports, 40 (7), https://doi.org/10.1016/j.celrep.2022.111182.

Persistent Link:
https://hdl.handle.net/11343/322102

Cell Reports

Article

Inhibition of mutant IDH1 promotes cycling of acute myeloid leukemia stem cells

Graphical abstract

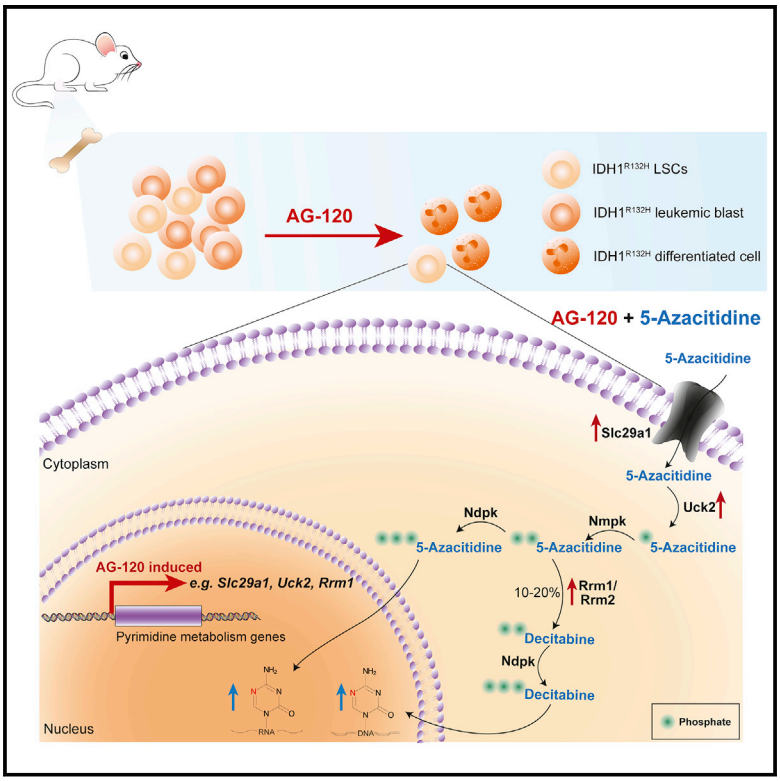

Highlights

- Inhibition of mutant IDH1 promotes exhaustion of the leukemic hierarchy
- Resistance to the IDH1 inhibitor AG-120 can arise through transcriptional reprogramming
- The differentiation state of AML cells affects their response to IDH1 inhibition
- The response of LSCs to AG-120 sensitizes them to azacitidine

Authors

Emily Gruber, Joan So, Alexander C. Lewis, ..., Jake Shortt, Ricky W. Johnstone, Lev M. Kats

Correspondence

lev.kats@petermac.org

In brief

IDH1-mutant acute myeloid leukemia cells accumulate the oncometabolite D-2-hydroxyglutarate (2-HG). Gruber et al. demonstrate that pharmacological 2-HG blockade sensitizes rare leukemia stem cells to the cytosine analogue azacitidine by promoting cycling and upregulating pyrimidine salvage.

Gruber et al., 2022, Cell Reports *40*, 111182
August 16, 2022
https://doi.org/10.1016/j.celrep.2022.111182

CellPress

Cell Reports

CellPress
OPEN ACCESS

Article

Inhibition of mutant IDH1 promotes cycling of acute myeloid leukemia stem cells

Emily Gruber,[1] Joan So,[1,2] Alexander C. Lewis,[1] Rheana Franich,[1] Rachel Cole,[1] Luciano G. Martelotto,[3] Amy J. Rogers,[1] Eva Vidacs,[1] Peter Fraser,[1] Kym Stanley,[1] Lisa Jones,[1] Anna Trigos,[1] Niko Thio,[1] Jason Li,[1] Brandon Nicolay,[4,8] Scott Daigle,[4,5] Adriana E. Tron,[4,5] Marc L. Hyer,[4,5,9] Jake Shortt,[1,2,6,7] Ricky W. Johnstone,[1,2] and Lev M. Kats[1,2,10,*]

[1]The Peter MacCallum Cancer Centre, Melbourne, VIC 3000, Australia
[2]The Sir Peter MacCallum Department of Oncology, University of Melbourne, Parkville, VIC 3052, Australia
[3]The University of Melbourne Centre for Cancer Research, The University of Melbourne, Parkville, VIC 3052, Australia
[4]Agios Pharmaceuticals, Inc., Cambridge, MA 02139, USA
[5]Servier Pharmaceuticals, Boston, MA 02210, USA
[6]School of Clinical Sciences at Monash Health, Monash University, Clayton, VIC 3068, Australia
[7]Monash Haematology, Monash Health, Clayton, VIC 3068, Australia
[8]Present address: Cedilla Therapeutics, Cambridge, MA 02142, USA
[9]Present address: Repare Therapeutics, Montreal, QC H4S 2A1, Canada
[10]Lead contact
*Correspondence: lev.kats@petermac.org
https://doi.org/10.1016/j.celrep.2022.111182

SUMMARY

Approximately 20% of acute myeloid leukemia (AML) patients carry mutations in IDH1 or IDH2 that result in over-production of the oncometabolite D-2-hydroxyglutarate (2-HG). Small molecule inhibitors that block 2-HG synthesis can induce complete morphological remission; however, almost all patients eventually acquire drug resistance and relapse. Using a multi-allelic mouse model of IDH1-mutant AML, we demonstrate that the clinical IDH1 inhibitor AG-120 (ivosidenib) exerts cell-type-dependent effects on leukemic cells, promoting delayed disease regression. Although single-agent AG-120 treatment does not fully eradicate the disease, it increases cycling of rare leukemia stem cells and triggers transcriptional upregulation of the pyrimidine salvage pathway. Accordingly, AG-120 sensitizes IDH1-mutant AML to azacitidine, with the combination of AG-120 and azacitidine showing vastly improved efficacy *in vivo*. Our data highlight the impact of non-genetic heterogeneity on treatment response and provide a mechanistic rationale for the observed combinatorial effect of AG-120 and azacitidine in patients.

INTRODUCTION

Acute myeloid leukemia (AML) is a low-survival cancer with a 5-year overall survival rate that still languishes below 30%. As is the case with normal hematopoiesis, AML cells are organized in a developmental hierarchy that partially recapitulates myeloid differentiation. At the apex of the hierarchy are rare leukemia stem cells (LSCs) that share many properties of hematopoietic stem cells (HSCs), including similar gene expression programs and capacity for self-renewal. LSCs in turn give rise to "bulk" tumor cells that have limited proliferative capacity but are not fully differentiated and exert pathologic effects on their microenvironment (Bonnet and Dick, 1997; van Galen et al., 2019). This non-genetic heterogeneity is a significant challenge for therapeutic targeting and the inability to fully eliminate LSCs has been linked with poor outcomes in model systems and AML patients (Fong et al., 2015; Ng et al., 2016).

Recurrent mutations in *IDH1* and *IDH2* genes were initially uncovered by cancer genome sequencing projects more than a decade ago and occur in approximately 20% of AML as well as a range of other cancers (Mardis et al., 2009; Parsons et al., 2008). Mutations are typically heterozygous and affect arginine residues within the enzymatic active site, most commonly R132 of IDH1 or R140/R172 of IDH2 (Papaemmanuil et al., 2016). Mutant IDH proteins possess a neomorphic enzymatic activity, reducing α-ketoglutarate (α-KG) to the rare but structurally similar metabolite D-2-hydroxyglutarate (2-HG) (Dang et al., 2009). 2-HG accumulates to millimolar concentrations in IDH-mutant cells and has been shown to deregulate α-KG-dependent pathways in a cell context-dependent manner. Critical cancer-associated proteins that are affected by 2-HG include the TET family of enzymes, which mediate DNA demethylation; the JmjC domain-containing histone demethylases; propyl hydroxylases, which regulate hypoxic signaling and collagen maturation; and the BCAT1/2 transaminases, which catalyze the synthesis of branched-chain amino acids (Figueroa et al., 2010; Koivunen et al., 2012; McBrayer et al., 2018; Sasaki et al., 2012a; Xu et al., 2011).

Multiple studies have confirmed mutant IDH1/2 as *bona fide* oncogenes. IDH mutations confer anchorage and cytokine-independent growth in various cell types *in vitro* and co-operate with

additional genetic lesions to initiate cancer *in vivo* (Chen et al., 2013; Kats et al., 2014; Losman et al., 2013; Lu et al., 2012). Extensive pre-clinical evidence supports the notion that mutant IDH proteins are highly promising drug targets in AML. First and foremost, IDH-mutant cells demonstrate an oncogene-addicted phenotype, at least in some genetic settings. Pharmacological inhibition of 2-HG production or genetic depletion of mutant IDH can abrogate *in vitro* surrogates of transformation such as colony formation and cytokine independence, and critically reduce disease burden *in vivo* in mouse models (Kats et al., 2014, 2017; Losman et al., 2013; Shih et al., 2017). As mutant IDH enzymes possess a neomorphic biochemical activity, this putatively provides a wide therapeutic window for targeting malignant cells without affecting normal tissues. Additionally, as 2-HG is readily detectable in the serum of AML patients, it serves as a useful biomarker of pharmacodynamic efficacy (Amatangelo et al., 2017). Finally, deep sequencing and single-cell studies designed to detect clonal architecture have shown that IDH mutation is an early event in leukemia evolution and is present in all or the vast majority of AML cells (Miles et al., 2020; Papaemmanuil et al., 2016; Quek et al., 2018).

In the past 5 years, inhibitors of mutant IDH proteins have entered clinical use, demonstrating ~40% overall response rate in relapsed-refractory AML as single agents (Amatangelo et al., 2017; DiNardo et al., 2018). Responses to these drugs are broadly associated with differentiation of leukemic blasts, consistent with the known effect of 2-HG on myeloid development (Kats et al., 2014; Sasaki et al., 2012b). Notably, however, the cellular and molecular details of the impact of IDH inhibition on the malignant hierarchy remain incompletely understood. Moreover, although some patients achieve complete morphological remission, almost all eventually relapse, with the majority of cases retaining expression of the mutant IDH allele and effective blockade of 2-HG production by the inhibitor (Choe et al., 2020; Quek et al., 2018). These observations suggest that a small population of IDH-mutant malignant cells with the properties of LSCs can persist during treatment and serve as the reservoir for relapse.

Herein, we developed a novel inducible mouse model of IDH1-mutant AML that enabled us to study the response of different malignant cell types to the IDH1 inhibitor AG-120 (ivosidenib). By leveraging single-cell transcriptomics, we provide insights into non-genetic heterogeneity in AML and identify a novel pathway to target LSCs.

RESULTS

Development of a multigenic AML model with inducible expression of IDH1^{R132H}

To explore the role of mutant IDH1 in leukemia maintenance *in vivo*, we developed a novel mouse model termed I1DN using a methodology that we had previously applied to study mutant IDH2 (Kats et al., 2017). I1DN tumors were generated by co-transduction of fetal liver-derived hematopoietic stem and progenitor cells (HSPCs) with three retroviral vectors encoding a doxycycline (dox)-regulated *IDH1*^{R132H} allele linked to a dsRed fluorescent reporter, and constitutive *DNMT3A*^{R882H} and *NRAS*^{G12D} alleles linked to GFP and a tetracycline transactivator (tTA), respectively (Figure 1A). Importantly, this triple-mutant combination is among the most prevalent in IDH1-mutant AML, and recent single-cell DNA sequencing analyses have confirmed that the mutations co-occur in individual leukemic cells (Cancer Genome Atlas Research Network et al., 2013; Miles et al., 2020; Morita et al., 2020; Papaemmanuil et al., 2016). Primary recipient mice transplanted with co-transduced HSPCs succumbed to a lethal myeloid leukemia characterized by splenomegaly and leukocytosis within 5–9 weeks (Figures 1B–1D). Consistent with functional co-operation between the three oncogenes, donor-derived cells in the peripheral blood, spleen, and bone marrow were almost exclusively GFP$^+$dsRed$^+$, even though this population represented only a fraction of the cells that were transplanted. Leukemic cells from primary recipients recapitulated disease in both syngeneic and immune-compromised NOD scid gamma (NSG) mice in serial transplants (Figures 1B and S1A). The expression of all three mutant proteins was further confirmed by western blotting, and liquid chromatography-mass spectrometry (LC-MS) analysis of plasma from moribund animals revealed the expected accumulation of 2-HG that was proportional to disease burden (Figures S1B and S1C). Administration of dox-supplemented food and water reduced expression of dsRed-linked IDH1^{R132H} in the bone marrow and spleen to near baseline levels within 5 days, whereas expression of GFP-linked DNMT3A^{R882H} and NRAS^{G12D} were maintained (Figures S1D–S1F).

Dysregulated differentiation is a classic feature of AML, with leukemic cells existing in a truncated developmental hierarchy dominated by an expansion of immature cells (Quek et al., 2018; van Galen et al., 2019). We used a comprehensive panel of cell surface markers and flow cytometry to quantify hematopoietic cell subsets within our model at advanced stage disease. A small proportion (5%–15%) of I1DN cells in the bone marrow and spleens of diseased mice expressed the stem-progenitor marker cKit, whereas the majority expressed the myeloid lineage marker CD11b (Figures 1E, 1F, and S1G). The cKit$^+$ population primarily encompassed cells with a committed myeloid progenitor-like immunophenotype and contained a mixture of common myeloid progenitors (CMPs; Lin$^-$Sca1$^-$cKit$^+$CD34$^+$FcγR^{int}) and granulocyte-macrophage progenitors (GMPs; Lin$^-$Sca1$^-$cKit$^+$CD34$^+$FcγR^{high}). The CD11b$^+$ population was predominantly marked by immature neutrophils with a striking block of differentiation from immature (Ly6G$^-$CD182$^-$) to mature (Ly6G$^+$CD182$^+$) neutrophils apparent in both organs (Figures 1E, 1F, and S1G) (Evrard et al., 2018). We performed a limiting dilution transplantation assay using the two most immature I1DN cell types, CMPs and GMPs (Figures S1H–S1J). Mice transplanted with sorted CMPs were the first to succumb to AML, with the disease phenotype indistinguishable from mice that were transplanted with unfractionated I1DN cells. There was a strong inverse correlation between the number of cells injected and disease latency. Eight-hundred CMPs were sufficient to initiate leukemia with 100% penetrance, whereas none of the mice injected with 800 GMPs developed disease, indicating at least a 10-fold enrichment in LSC frequency within the CMP compartment. In summary, we have developed a novel model of mutant IDH1 AML characterized by aberrant progenitor self-renewal

CellPress
OPEN ACCESS

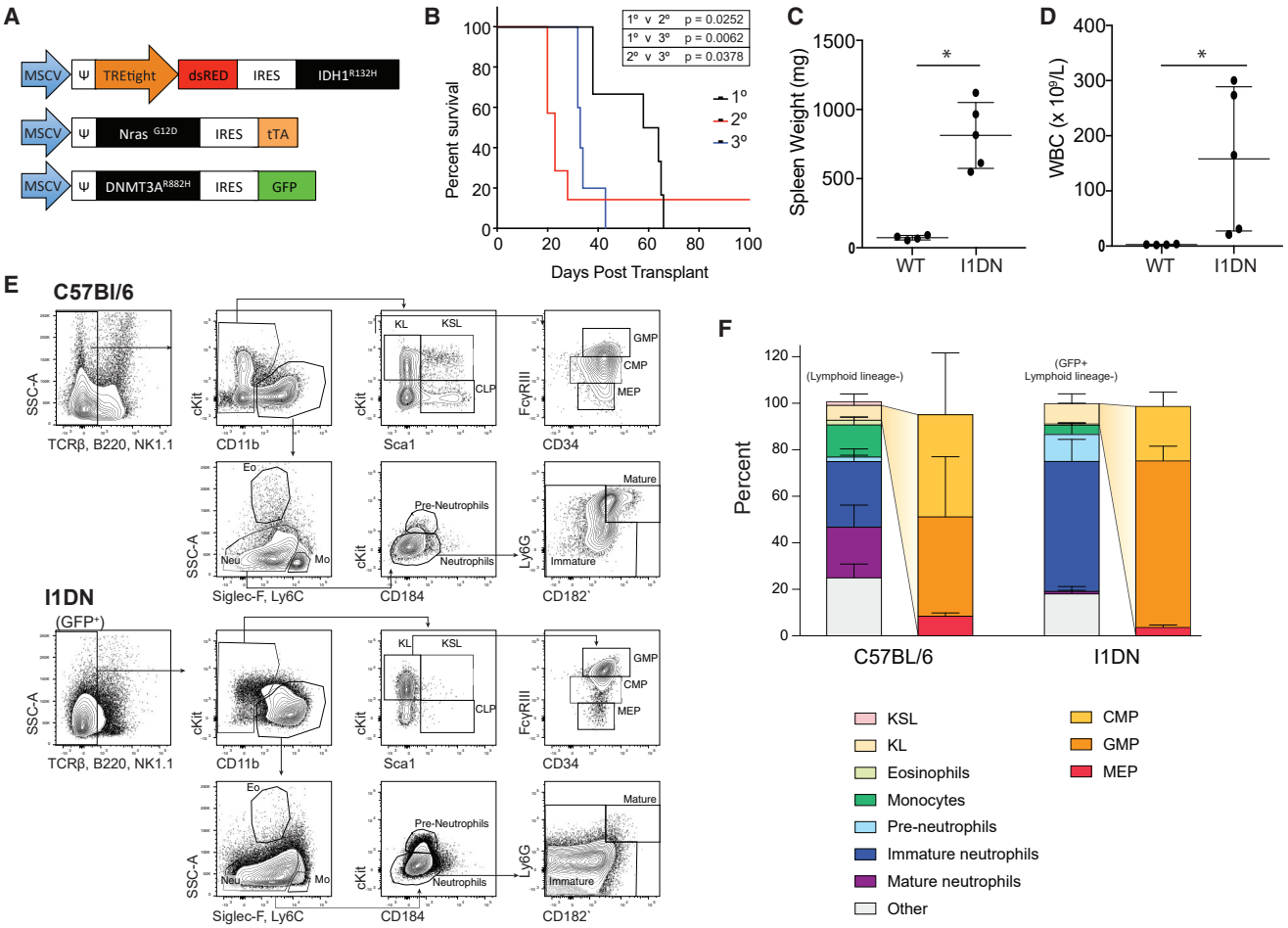

Figure 1. Co-expression of *IDH1*^{R132H}, *DNMT3A*^{R882H}, and *Nras*^{G12D} drives AML *in vivo*

(A) Schematic of retroviral constructs used to generate the I1DN model.

(B) Kaplan-Meier survival curve of mice transplanted with transduced hematopoietic stem and progenitor cells (HSPCs, 1° recipients), or with leukemic cells from spleen or bone marrow of moribund mice (2° and 3° recipients) (n = 5–6 mice/transplant).

(C and D) Spleen weight (C) and peripheral white blood cell counts (D) of 1° I1DN recipients or control C57BL/6 wild-type mice (n = 4–5; data represented as mean ± SD; p value was calculated by two-tailed, non-parametric student's t test; *p < 0.05).

(E) Representative FACS plots of myeloid progenitors and mature myeloid lineages present in the bone marrow of C57BL/6 mice and leukemic (GFP+) cells from moribund I1DN recipients.

(F) Bar graph of proportion of leukemic cell types from the bone marrow of moribund I1DN-transplanted mice.

and a block of myeloid differentiation at the immature neutrophil stage.

Inhibition of mutant IDH1 promotes AML differentiation and prolongs survival

Small molecule inhibitors of mutant IDH proteins have demonstrated efficacy in model systems and clinical trials (DiNardo et al., 2018; Kats et al., 2017; Shih et al., 2017; Stein et al., 2017), but the molecular and cellular events downstream of 2-HG depletion remain incompletely understood. We used the I1DN model to assess the impact of IDH1 targeting *in vivo* and compared pharmacological inhibition by the clinical IDH1 inhibitor AG-120 (also called ivosidenib) with genetic depletion of the IDH1^{R132H} transgene. We first confirmed that AG-120 therapy reduced 2-HG in the plasma and bone marrow of leukemic mice, as expected (Figure S2A). We then treated a cohort of I1DN-engrafted recipients with vehicle, AG-120, or dox and monitored disease progression and survival (Figures 2A, S2B, and S2C). In the vehicle-treated group, the rapid increase in peripheral blood tumor burden was accompanied by the development of severe thrombocytopenia, with all animals requiring euthanasia due to AML by day 38 post transplant. By comparison, disease progression in AG-120 and dox-treated animals was arrested following 2–3 weeks of treatment, and although I1DN cells continued to be detectable for the duration of the study, platelet counts normalized. Ten out of 11 mice in the AG-120 group and 12 out of 12 mice in the dox group survived until day 42, at which point treatment was withdrawn to determine whether the disease relapsed. Surprisingly, tumor burden remained stable, although most

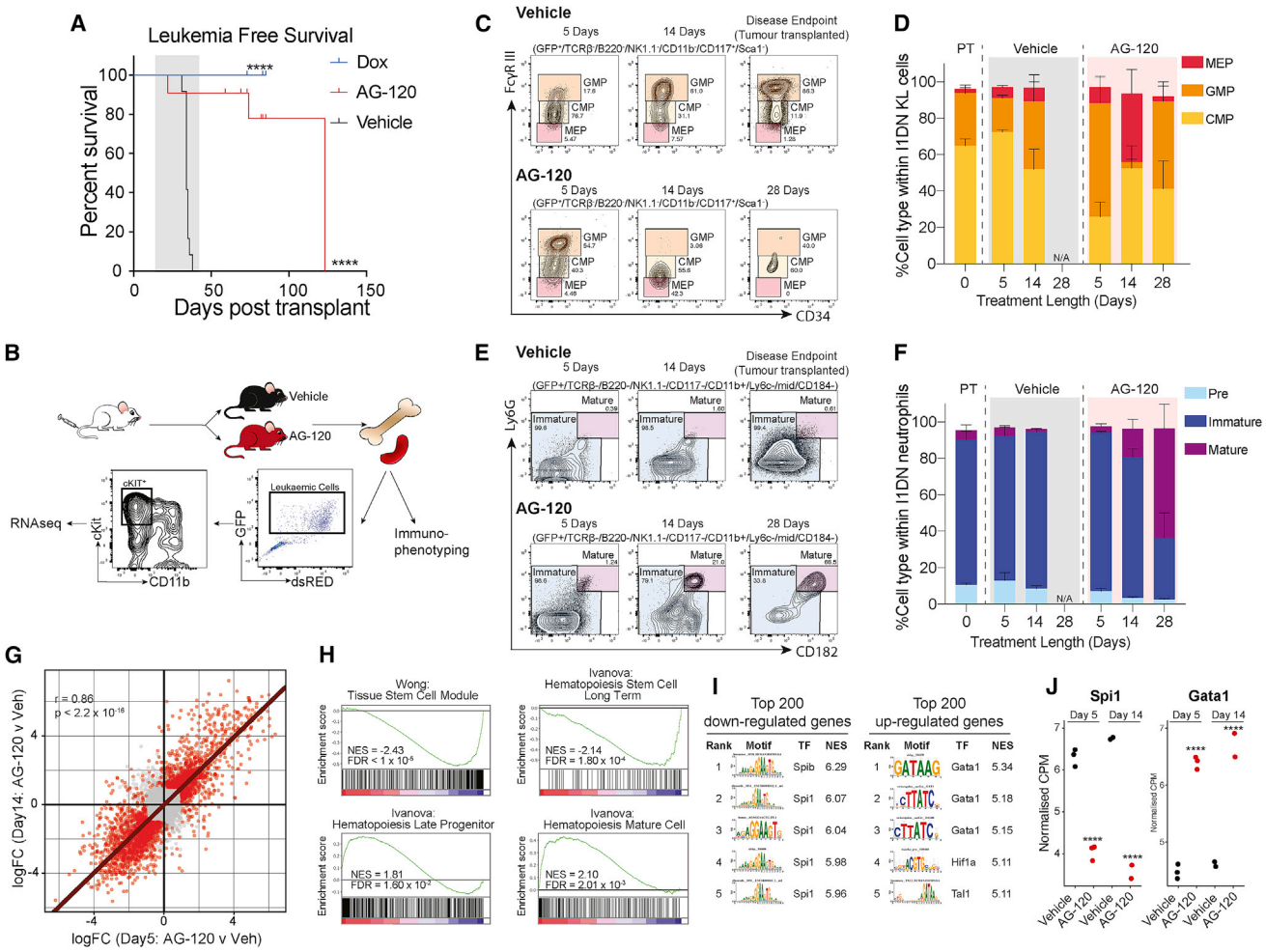

Figure 2. AG-120 promotes differentiation and delayed disease regression *in vivo* by depleting 2-HG

(A) Kaplan-Meier progression-free survival curve of I1DN tumor-bearing mice treated with AG-120, dox, or vehicle. Gray shading denotes treatment. Mice that succumbed to graft-versus-host disease were censored (n = 11–12 mice/group; p value was calculated by log rank test; ****p < 0.0001).

(B) Schematic of experimental design.

(C–F) Immunophenotype of I1DN leukemic cells in the bone marrow of mice treated with AG-120 or vehicle for the indicated time period. Representative FACS plots (C and E) and quantification (D and F) of the progenitor (C and D) and mature (E and F) leukemic compartments is shown (n = 3–4 mice/group/time point; data represented as mean ± SD).

(G–J) RNA-seq analysis of sorted I1DN progenitor cells. (G) Correlation plot of differentially expressed genes (DEGs) induced by AG-120 following 5 and 14 days of treatment. Red circles represent significant DEGs (FDR < 0.01 and |logFC| > 1) in either comparison. Line of best fit calculated for significant DEGs in either comparison.

(H) GSEA barcode plots showing downregulation of HSC-associated genes and upregulation of myeloid differentiation genes following 5 days of AG-120 treatment.

(I) Enrichment of transcription factor binding sites identified within the proximal promoters of the top 200 AG-120 up- or downregulated genes identified by RcisTarget. Ranking was determined by normalized enrichment score (NES).

(J) Normalized expression of *Spi1* and *Gata1* (****FDR < 0.0001 calculated with the limma package in R).

animals developed a graft-versus-host-disease-like condition (likely caused by co-transfer of a small number of T-cells; see Figure S2D; Table S1) and had to be withdrawn from the study, precluding long-term analysis. We did, however, identify at least two *bona fide* relapses in the AG-120 group (#13 and #23) characterized by rapid expansion of I1DN cells and coincidental onset of thrombocytopenia. Taken together, our findings demonstrate that IDH1 inhibition is effective *in vivo* against IDH1-mutant AML and confers a significant survival benefit in treated animals but does not fully eliminate the disease.

To characterize the impact of IDH1 inhibition on the AML hierarchy in greater detail, we analyzed additional cohorts of tumor-bearing mice that had been treated with vehicle or AG-120 for 5 days, or 2 or 4 weeks (the maximum allowable time under our approved animal ethics protocol) (Figure 2B). For these and subsequent experiments, we used I1DN tumors that had been depleted of lymphoid cells to reduce the incidence of

graft-versus-host disease (see STAR Methods). AG-120 initially increased the total tumor burden in the bone marrow and spleen, and at 5 days there was a dramatic increase in spleen size and macroscopically visible regions of dense blast cell infiltrate into the medulla of the spleen of treated animals compared with controls (Figures S2E and S2F). The initial burst of proliferation was later followed by disease regression, and, notably, the kinetics differed between different organs, with reduction of I1DN cells in the bone marrow and spleen preceding that in the peripheral blood. Flow cytometric analysis revealed progressive myeloid differentiation that was evident as early as 5 days after treatment initiation but continued to progress over 4 weeks (Figures 2C–2F). Initially, we observed changes predominantly in the immature cKit^{+}Lineage^{-} (KL) compartment (hereafter referred to as the progenitor compartment), with an increase in the GMP: CMP ratio. At later time points, these immature cells were almost completely eliminated, although a small population of CMPs remained at the end of treatment. Mature (cKit^{-}CD11b^{+}) cells continued to accumulate, eventually acquiring the phenotype of fully differentiated neutrophils. Taken together, our data suggest that AG-120 acts at multiple levels of the AML hierarchy, altering the phenotypes of both LSCs and bulk tumor cells, leading to exhaustion and delayed tumor regression (Figure S2G).

We next analyzed the impact of IDH1 inhibition on gene expression by RNA sequencing (RNA-seq) of sorted leukemic progenitor cells from I1DN tumor-bearing mice that had been treated with vehicle or AG-120 for 5 or 14 days (Figure 2B). We identified 2,207 and 2,211 differentially expressed genes (DEGs; false discovery rate [FDR] <0.01, and $|\log_2 FC| > 1$) following 5 and 14 days of AG-120 treatment, respectively (Table S2). Transcriptional alterations at the two time points were highly positively correlated, demonstrating that AG-120-induced changes can occur within days of treatment initiation and remain stable over time (Figures 2G and S2H). Among the DEGs shared between 5 and 14 days of drug treatment were numerous factors with well-known roles in normal and malignant hematopoiesis. These included *Meis1*, *Sox4*, and *S1pr1*, which were downregulated (Table S2). *Meis1* and *Sox4* encode stem cell-associated transcription factors that are frequently dysregulated in AML and contribute to increased self-renewal capabilities that drive uncontrolled proliferation (Wang et al., 2005; Zhang et al., 2013), whereas *S1pr1* regulates egress of lineage committed HSPCs from the bone marrow into the blood (Juarez et al., 2012). On the other hand, *Prg2* and *CD177*, which have functions in mature myeloid cells, were upregulated. Unbiased analysis using gene set enrichment analysis (GSEA) (Subramanian et al., 2005) further confirmed a strong negative enrichment of HSPC-associated gene sets and, conversely, a strong positive enrichment of gene sets that govern myeloid differentiation (Figure 2H). Furthermore, using the RcisTarget algorithm, we identified the Gata1/Spi1 axis as a potent driver of the AG-120 response. Gata1 and Spi1 are cross-antagonistic transcription factors that inhibit each other's activity while promoting their own (Hoppe et al., 2016). Gata1 and Spi1 binding motifs were highly over-represented in the most significant AG-120 up- and downregulated genes, respectively (Figure 2I). Concordantly, *Gata1* expression was increased while *Spi1* expression was reduced (Figure 2J). Thus, IDH1 inhibition alters the expression of molecular programs that control self-renewal and differentiation.

The oncometabolite 2-HG has been postulated as the primary effector through which mutant IDH proteins exert their oncogenic function (Kats et al., 2017; Koivunen et al., 2012; Losman et al., 2013). Notably, recent studies have implicated the reacquisition of 2-HG production via alternative pathways as a mechanism driving resistance to IDH inhibitor therapy in a subset of AML patients (Harding et al., 2018; Intlekofer et al., 2018; Morita et al., 2020). We compared the AG-120 transcriptional signature with a signature of mutant IDH2 inhibition that we had previously derived in an isogenic AML model driven by IDH2^{R140Q}, DNMT3A^{R882H}, and Nras^{G12D} (Kats et al., 2017). Using rotating gene set testing (ROAST) (Wu et al., 2010), we identified significant enrichment of DEGs that were perturbed by IDH2^{R140Q} inhibition in the AG-120 transcriptional signature (Figure S2I). We directly compared the effects of AG-120 and deinduction of the IDH1^{R132H} transgene by dox and found that both treatments elicited phenotypic differentiation of I1DN progenitors and highly similar gene expression changes by RNA-seq (Figures S2J and S2K). Taken together, these data demonstrate that the effects of AG-120 are mediated by on-target inhibition of 2-HG production.

Resistance to IDH inhibition is associated with transcriptional reprogramming

Our initial survival study prompted us to explore whether I1DN leukemic mice that had relapsed after treatment withdrawal developed AG-120-resistant disease. The cross-sectional study shown in Figures 2B–2J also included a cohort of tumor-bearing mice treated with AG-120 for 4 weeks and subsequently monitored for disease relapse. We observed delayed disease regression in the peripheral blood of these animals (Figure S3A), but none attained complete remission and I1DN cells continued to be detectable in the peripheral blood by fluorescence-activated cell sorting (FACS). Notably, the greatest reduction in peripheral blood tumor burden occurred after treatment withdrawal, demonstrating the lag between IDH inhibition and disease regression that likely occurs due to the time required for LSCs to differentiate. In all four mice, disease remained stable for at least 6 weeks before relapse. The kinetics of relapse strongly suggest that I1DN cells had remained latent for several weeks after treatment cessation before reacquiring proliferative capabilities.

To gain insights into gene expression programs that may underpin the relapse in these I1DN tumors, hereafter referred to as treatment-exposed (TE) leukemias, we compared the transcriptome of the I1DN TE progenitors and I1DN vehicle-treated progenitors. In multidimensional scaling (MDS) analysis, I1DN TE samples formed two distinct clusters and were separated from vehicle-treated samples, indicating the establishment of novel transcriptional states in relapsed leukemias (Figure 3A). We combined the two samples in each cluster (TE1 and TE2) and then identified DEGs between TE clusters and vehicle-treated samples. Overall, there were 687 and 897 DEGs (FDR < 0.05 and $|\log_2 FC| > 0.5$) between TE1 or TE2 and vehicle treated, respectively, with few overlapping DEGs between TE1 and TE2 (Figures 3B and S3B; Table S2). GSEA and Gene

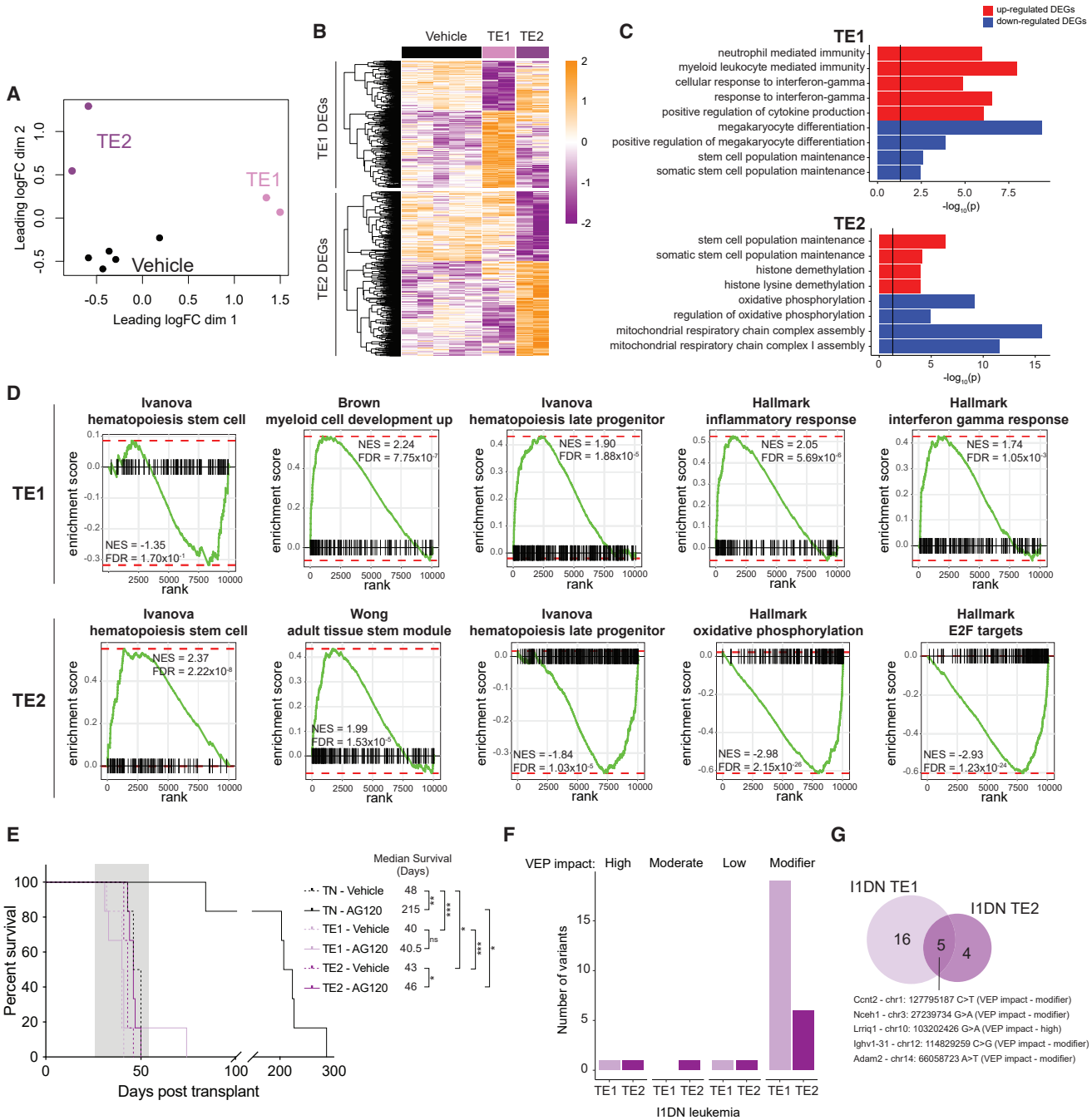

Figure 3. I1DN tumors resistant to AG-120 are characterized by altered gene expression

(A–D) RNA-seq of cKit+ I1DN progenitor cells from vehicle-treated mice or AG-120 relapsed mice. (A) MDS plot of the top 500 most variably expressed genes. (B) Heatmap of TE1 and TE2 DEGs (FDR < 0.05 and |logFC| > 0.5). (C) Gene Ontology (GO) terms of TE1 and TE2 DEGs. (D) GSEA pathways of TE1 and TE2 DEGs. (E) Kaplan-Meier survival curve of mice transplanted with I1DN treatment-naive (TN) or treatment-exposed (TE) leukemias and treated with AG-120 or vehicle (n = 6 mice/group; p value was calculated by log rank test; *p < 0.05, **p < 0.01, ***p < 0.001).

(F) Number of variants detected by exome sequencing.

(G) Venn diagram of the variants detected in each TE leukemia.

Ontology (GO) analyses revealed that TE1 was characterized by the upregulation of myeloid differentiation and inflammatory gene sets, whereas TE2 tumors upregulated stem cell and histone methylation pathways while downregulating mitochondrial respiratory and oxidative phosphorylation signatures (Figures 3C and 3D). RcisTarget identified Spi1 and Foxo1 as

the top transcription factor motifs upstream of upregulated TE1 and TE2 DEGs, respectively (Figure S3C).

To determine whether relapsed I1DN TE tumors had acquired resistance to IDH1 inhibition, we transplanted cells from two mice (TE1, mouse #24; and TE2, mouse #23) into cohorts of secondary recipients. We also transplanted mice with I1DN treatment-naive (TN) cells. Concordant with our previous studies, AG-120 prolonged survival in the TN cohort, whereas mice transplanted with TE cells did not respond to AG-120 (Figure 3E). Of note, although the median survival of all vehicle-treated cohorts differed by less than 7 days, it was slightly lower in both TE cohorts, suggesting that these tumors proliferate more rapidly at baseline.

We performed exome sequencing on a TE1 tumor, a TE2 tumor, and a TN tumor (Figures 3F and 3G). Comparison of the mutational profiles identified only a single mutation in *Lrriq1* that was predicted to have a detrimental effect on protein function as determined by the Variant Effect Predictor functional consequence rank. *Lrriq1* expression was undetectable in I1DN progenitor cells by RNA-seq. No mutations were identified in hematopoietic transcription factor or kinase signaling genes. Mutant isoform switching and gate-keeper mutations in IDH1 and -2 have been observed in a proportion of AML patients with acquired resistance to IDH inhibitors (Harding et al., 2018; Intlekofer et al., 2018). Close examination of the IDH1 and -2 loci revealed no mutations within the coding domain sequences of these genes, including the recurrently mutated hotspot codons. These findings suggest that the drug-resistant and transcriptional phenotypes of I1DN TE tumors are the result of epigenetic rather than genetic changes.

AG-120 promotes cycling of quiescent LSCs and upregulates the pyrimidine salvage pathway

Over the past decade, it has become apparent that non-genetic drivers underpin a large proportion of functional variation in cancer, including the capacity of rare cell populations to withstand therapeutic pressure ultimately leading to drug resistance (Marine et al., 2020). To investigate the extent of heterogeneity of AG-120 transcriptional responses, we utilized the 10X Genomics 3′ single-cell RNA-seq (scRNA-seq) platform to profile gene expression from individual I1DN progenitor cells isolated from mice following 5 days of inhibitor or vehicle treatment. After filtering, we obtained high-quality data for 7,708 cells with a median of 4,126 genes quantified per cell. Uniform manifold approximation and projection (UMAP) clustering identified nine distinct transcriptional clusters (Figures S4A and S4B), all of which contained cells from both vehicle- and AG-120-treated animals, suggesting that the grouping reflected the presence of different cellular states and was not based on the molecular response to IDH inhibition (Butler et al., 2018). Correlation analysis enabled us to merge clusters that had fewer than 100 cells to highly similar larger clusters, generating seven main progenitor groups (Figure 4A).

Each group expressed distinct patterns of well-established hematopoietic differentiation markers (Lara-Astiaso et al., 2014) that led us to annotate group 5 as GMP-like (high expression of *Fcgr3* and *Mpo*), groups 6 and 7 as MEP-like (high expression of *CD71* and *Klf1*), group 1 as LSCs (high expression of *Erg*, *Junb*, and *Sox4*), and groups 2–4 as intermediate (Figures 4B and 4C). Concordant with our manual annotation, cells within group 7 upregulated expression of genes required for heme biosynthesis, whereas group 5 was marked by signatures of myeloid cell activation and groups 1–4 by various stemness associated signatures (Figure 4D). Notably, group 1 cells most closely resembled long-term HSCs, as shown by their high hscScore (Hamey and Göttgens, 2019) and prominent expression of the "low-output" signature characteristic of quiescent, self-renewing, long-term repopulating HSCs recently identified through lineage tracing experiments that coupled barcoding and scRNA-seq (Rodriguez-Fraticelli et al., 2020) (Figures 4E, 4F, and S4C). Group 1 also displayed high expression of LSC17 genes, a signature derived from functional LSCs isolated from AML patients that predicts poor clinical outcome (Ng et al., 2016) (Figures 4F and S4C). Taken together, these analyses suggest that group 1 cells possess the highest LSC potential within the I1DN progenitor compartment.

We next analyzed the impact of AG-120 on the relative proportion of cells within each group (Figure S5A). As expected from our FACS and morphological observations, AG-120 treatment reduced the fraction of immature cells and conversely increased the abundance of more differentiated cells (Figures S5A and S5B). Analysis of cell cycle stage inferred from gene expression revealed that AG-120 also greatly increased the percentage of cycling cells, including within the putative LSC group 1 (Figure S5C) (Tirosh et al., 2016). Notably, in both HSCs and LSCs, loss of quiescence is linked with stem cell exhaustion (Lechman et al., 2016; Rodriguez-Fraticelli et al., 2020), suggesting that delayed tumor regression observed in AG-120-treated mice is underpinned by a collapse of the malignant hierarchy caused by depletion of functional LSCs.

Many studies have characterized the molecular responses of AML cells to various targeted agents, including IDH inhibitors (Choe et al., 2020; Kats et al., 2017; Shih et al., 2017). What remains unclear, however, is to what extent the differentiation state of a malignant cell affects its transcriptional response to treatment. To address this question and to understand the effects of AG-120 on different cell types, we performed differential gene expression within each progenitor group. This analysis identified partial overlap but also extensive heterogeneity of transcriptional responses, both at the level of individual genes and biological pathways (Figures 5A–5C and S5D–F). The transcriptomes of some cell types were more profoundly affected by AG-120 than others, as indicated by the number of DEGs that reached statistical thresholds (Figure S5D). DEGs and signatures related to differentiation that were also evident in bulk RNA-seq (Figure 2) were enriched in almost all groups (5C and S5E). In contrast, most progenitor group-specific DEGs that were selectively perturbed only in individual cell types were not detected as differentially expressed in the bulk sequencing data (Figure S5F; Table S3). Cell cycle and proliferation-related signatures were much more strongly upregulated in group 1 cells; and interferon-α and apoptosis signatures were upregulated by AG-120 treatment in some cell types and downregulated in others (Figure 5C). These findings highlight the impact of transcriptional differences between genetically identical leukemic cells on their response to therapy.

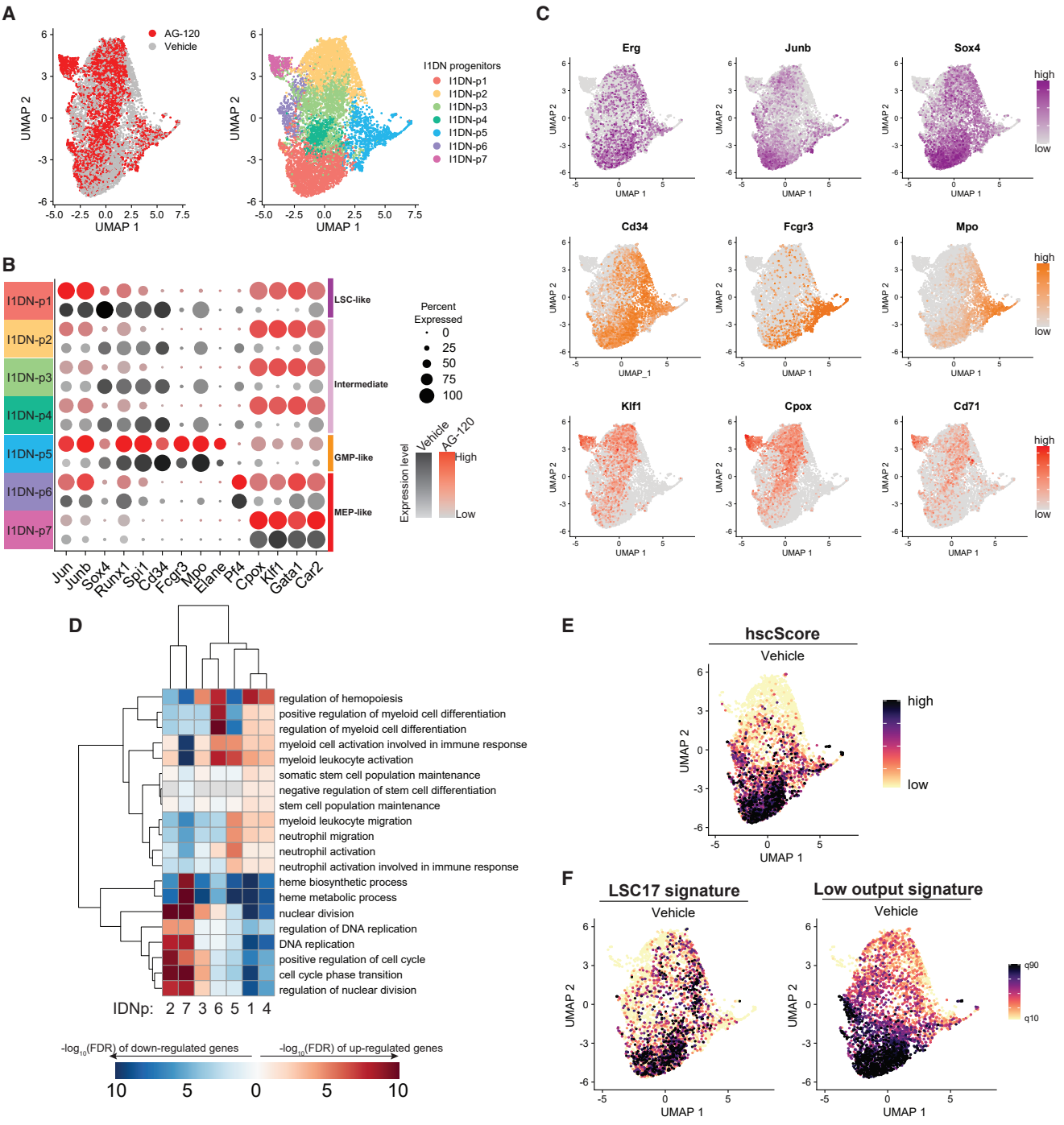

Figure 4. scRNA-seq identifies LSCs within the I1DN progenitor population

(A) I1DN progenitor cells from mice treated with AG-120 or vehicle for 5 days were analyzed by scRNA-seq. UMAP plot of integrated datasets labeled by treatment (left) or I1DNprogenitor (I1DN-p) group (right).

(B) Dot plot of gene expression across I1DNp groups and treatment.

(C) UMAP plots of highlighted genes.

(D) Heatmap of GO terms associated with genes significantly differentially expressed between the different ID1Np groups. Only cells from vehicle-treated mice were used in this analysis.

(E and F) UMAP plot of (E) hscScore (Hamey and Göttgens, 2019), (F) "low-output" HSC signature (Rodriguez-Fraticelli et al., 2020), and LSC17 gene expression (Ng et al., 2016). GMP, granulocyte-macrophage progenitor; MEP, megakaryocyte-erythroid progenitor.

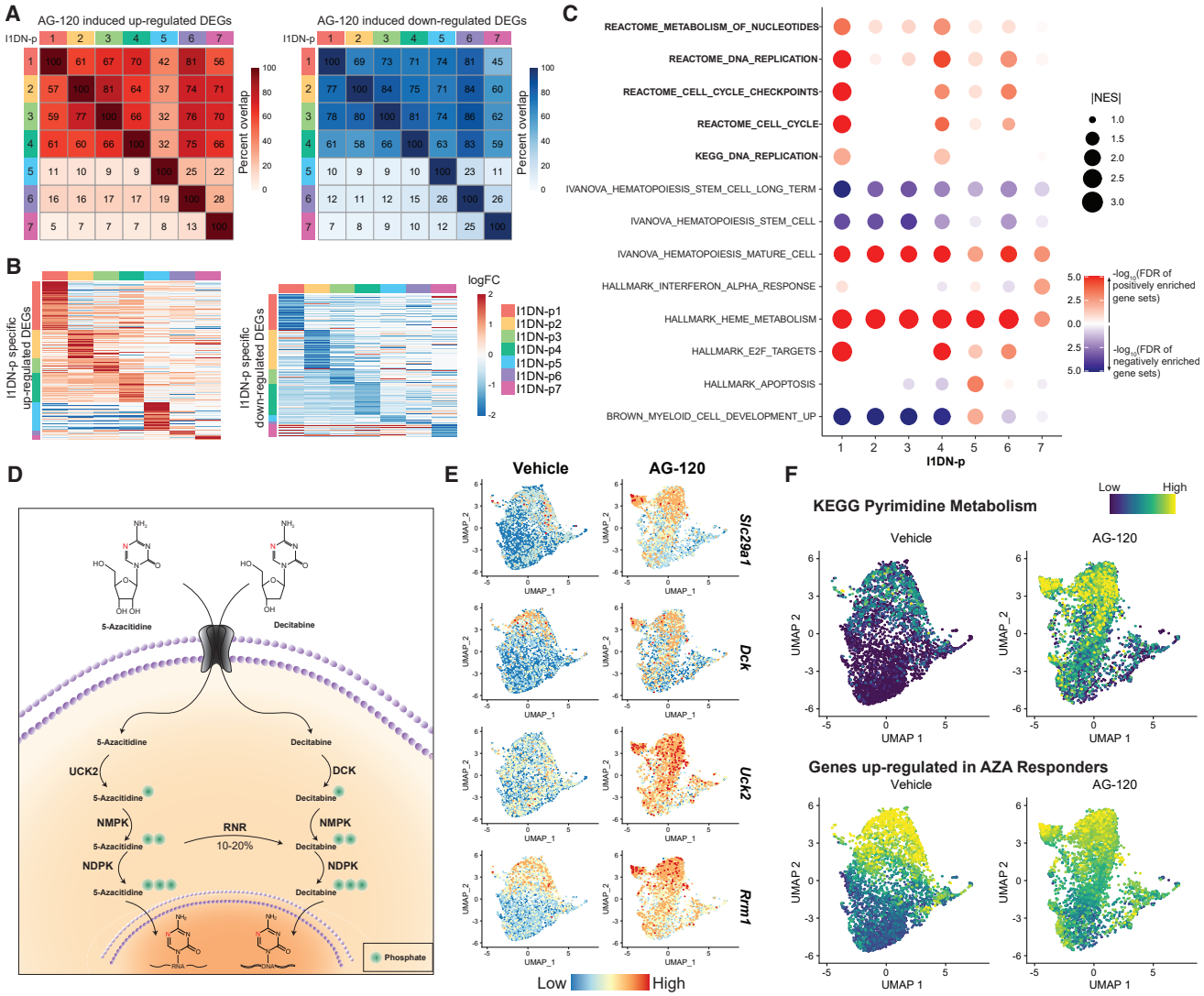

Figure 5. 2-HG blockade promotes LSC cycling and upregulation of the pyrimidine salvage pathway

(A) Heatmap of the percentage of overlap between the significantly up- (left) or downregulated (right) DEGs induced by AG-120 across each I1DN-p group. Percentage overlap was calculated with respect to each column group.

(B) Heatmap of cluster specific genes that were up- (left) or downregulated (right) by AG-120 in different I1DN-p groups.

(C) Dot plot depicting GSEA signatures enriched upon AG-120 treatment across each I1DNp group.

(D) Schematic showing the metabolism of hypomethylating agents azacitidine and decitabine.

(E) UMAP plot of the expression of specific genes involved in the metabolism of HMAs.

(F) UMAP plot of the average expression of the Kyoto Encyclopedia of Genes and Genomes (KEGG) pyrimidine metabolism signature and genes upregulated in azacitidine-responder patients (Unnikrishnan et al., 2017).

We then asked whether AG-120-induced transcriptional changes are likely to sensitize AML cells and, in particular, the LSC compartment to other known therapeutic agents, thereby providing an opportunity for a rationally designed combination strategy. Hypomethylating agents (HMAs) have been proposed as potential combination partners for IDH inhibitors on the basis that the two drug classes promote loss of DNA methylation via distinct pathways (MacBeth et al., 2021). Clinically utilized HMAs such as azacitidine and decitabine are nucleoside analogues that require DNA replication and enzymes of the pyrimidine salvage pathway for DNA incorporation in order to exert their anti-leukemic effects (Gruber et al., 2020; Gu et al., 2020). In addition to promoting the cycling of quiescent cells, AG-120 also increased expression of pyrimidine metabolism genes that are essential for HMA efficacy, including the equilibrative nucleoside transporter SLC29A1, the kinases UCK2 and DCK, and the ribonucleotide reductase subunit RRM1 (Figures 5D–5F and S5G–S5I) (Gruber et al., 2020; Gu et al., 2020). Of note, UCK2 and RRM1, which are required for azacitidine activity, were more significantly upregulated than DCK, which is needed for

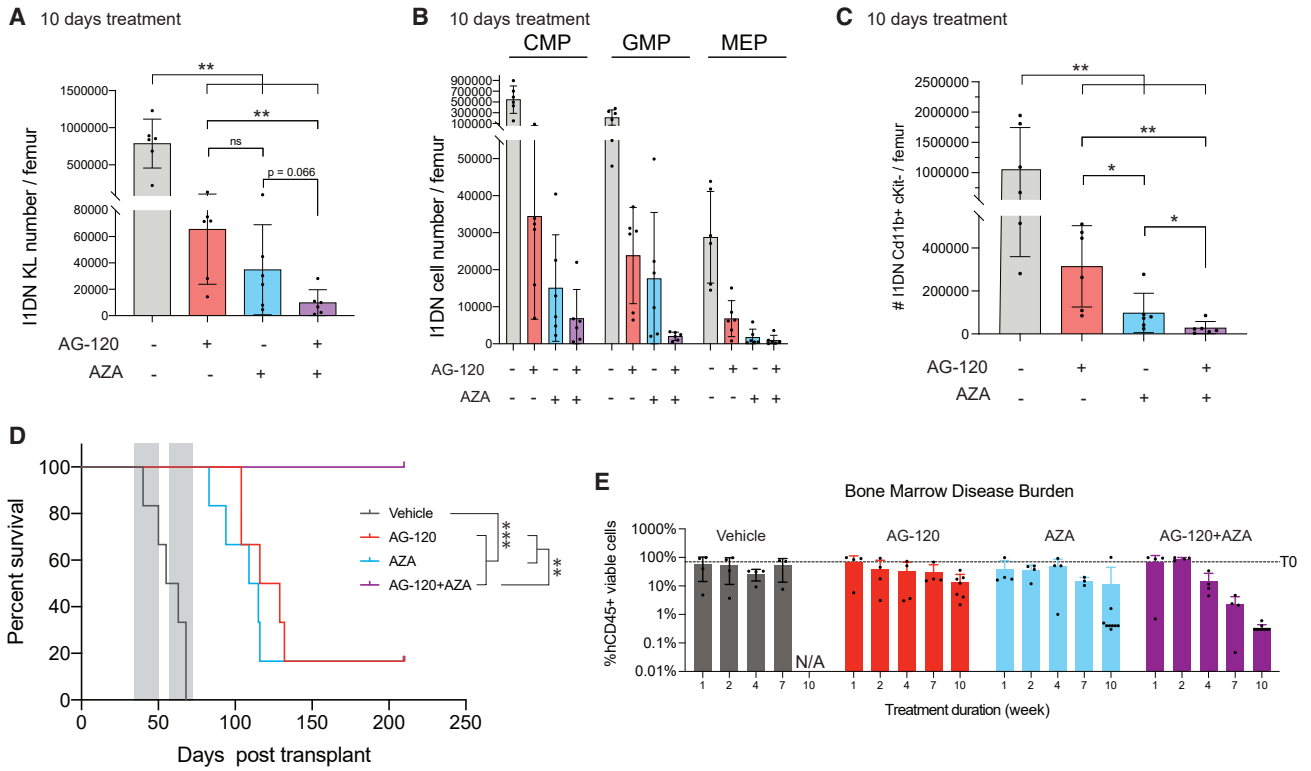

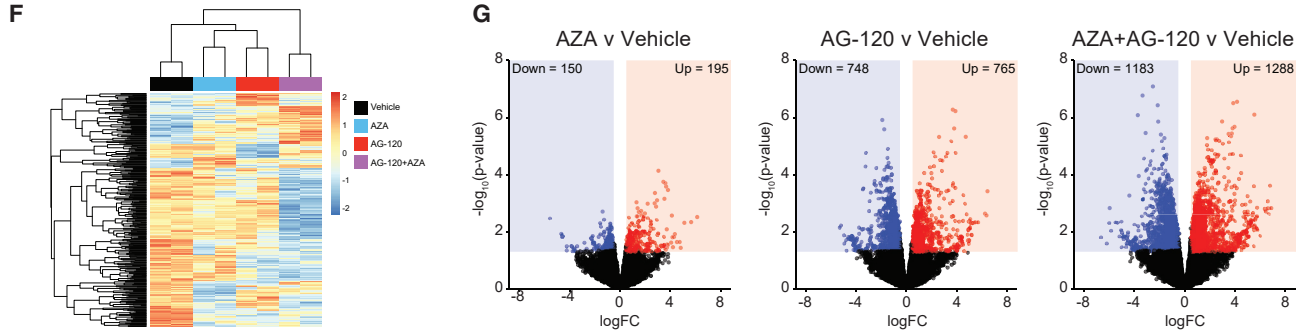

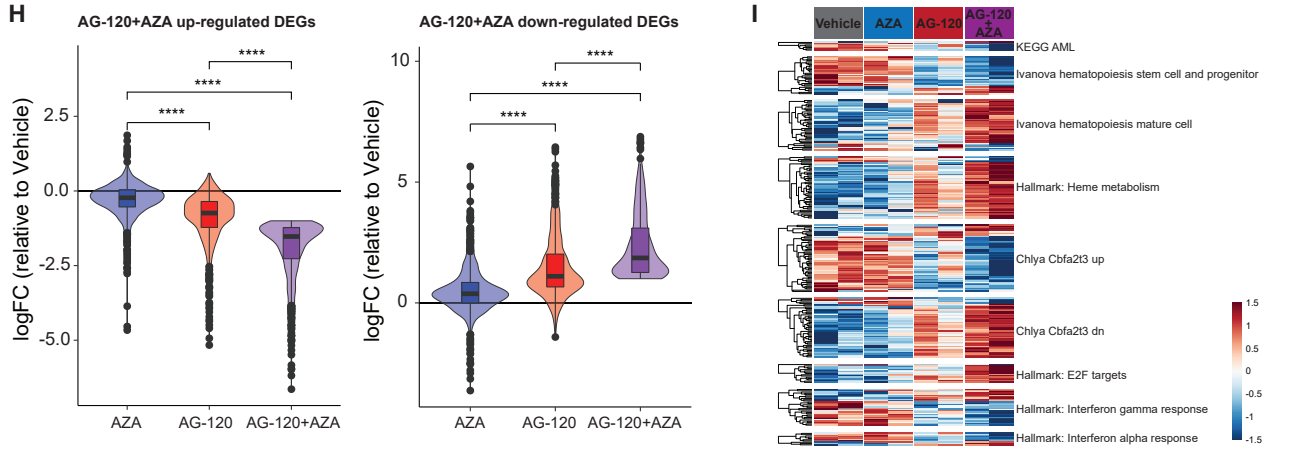

(legend on next page)

decitabine (Figure S5I). Furthermore, an unbiased transcriptional signature of HMA sensitivity derived by comparing HSPCs from myelodysplasia patients that responded or were refractory to azacitidine treatment (Unnikrishnan et al., 2017) was also prominently upregulated in AG-120-treated cells, including the I1DN progenitor group 1 cells (Figures 5F and S5H).

Regulation of pyrimidine metabolism has previously been linked with cell cycle and differentiation (Lane and Fan, 2015). Using publicly available RNA-seq data from studies that profiled normal blood development in mice (Lara-Astiaso et al., 2014) and humans (Rapin et al., 2014), we found that the expression of pyrimidine metabolism genes increases during differentiation of HSCs to committed myeloid progenitors (Figure S5J). Taken together, our results suggest that IDH inhibitors and HMAs, particularly azacitidine, are likely to synergize and promote the elimination of quiescent LSCs, leading to deep and long-lasting remission.

AG-120 and azacitidine synergize to provide long-lasting disease control

To test the efficacy of the rationally designed combination of AG-120 and azacitidine, we first performed a cross-sectional study in I1DN tumor-bearing mice. We used a modified dosing schedule where AG-120 was administered once per day and azacitidine was administered once per day in cycles of 2 days on and 1 day off. Animals were treated with vehicle, single agents, or the combination, and disease progression was assessed on day 10. Consistent with the reported sensitivity of IDH-mutant cancer cells to HMA treatment (MacBeth et al., 2021), azacitidine reduced leukemic burden at levels comparable with AG-120. The combination treatment was most effective, reducing overall disease burden and targeting both the leukemic progenitor compartment and mature leukemic cells (Figures 6A–6C).

We next tested the impact of the single-agent and combination regimens on survival (Figure 6D). Tumor-bearing mice were treated for two 14-day cycles separated by a 7-day recovery period using the modified regimen and monitored for symptom onset and disease progression in the peripheral blood. All mice in the vehicle group reached ethical endpoint prior to the conclusion of cycle 2. As expected from the cross-sectional study, both AG-120 and azacitidine significantly increased survival, although most animals (5 out of 6) in the single-treatment arms eventually succumbed to AML. Conversely, all animals in the combination group showed long-term survival with disease control that was sustained for at least 22 weeks after treatment was withdrawn. In all six of these mice, FACS analysis of peripheral blood at the endpoint failed to detect any circulating I1DN cells, potentially suggesting that the animals were leukemia free.

To provide orthogonal validation and confirm the relevance of our findings to human AML, we next turned to an *IDH1*^{R132H} patient-derived xenograft (PDX) AML model that also carried mutations *NPM1*^{W288fs*12}, *DNMT3A*^{A571fs}, and *FLT3*^{ITD}. Mice were randomized to treatment cohorts and preassigned groups from each cohort were euthanized at 1, 2, 4, 7, or 10 weeks post enrollment, with the exception of the control group as remaining mice required termination after week 7 due to reaching ethical endpoint. Disease progression in the bone marrow was quantified by FACS using antibodies directed against human CD45 (hCD45). In this model too, the combination of AG-120 and azacitidine was highly efficacious, with all 10 mice analyzed at week 10 having <1% tumor burden (Figure 6E).

We next investigated the consequences of the combined AG-120 and azacitidine treatment on DNA methylation and gene expression using reduced representation bisulfite sequencing (RRBS) and RNA-seq. Azacitidine triggers global loss of DNA methylation via degradation of the maintenance DNA methyltransferase DNMT1, which depends on replication and is proportional to drug uptake and incorporation into DNA (Unnikrishnan et al., 2018). IDH inhibitors are also associated with DNA demethylation linked to de-repression of TET2, although the impact of these drugs is less pronounced and more variable, especially in a DNMT3A-mutant context (Wang et al., 2021). Moreover, analyses that do not enrich for specific cell types and/or are performed at late timepoints may be confounded by the effects of differentiation.

To capture the acute impact of treatment, we analyzed I1DN progenitors isolated from mice that had been treated for 5 days with vehicle, each single agent alone, or the combination (Figures S6A and S6B). As expected for RRBS, we observed greatest sequence coverage in CpG-rich regions (Figure S6C) (Akalin et al., 2012) and thus focused our analysis on comparing the methylation status of promoters. Azacitidine treatment resulted in the fewest differentially methylated promoter regions (FDR < 0.05, 46 out of 13,549 promoter DMRs) and had minimal impact on transcription (Figures 6F, 6G, and S6D). Indeed, under azacitidine treatment, no genes passed our stringent statistical thresholds (FDR < 0.05) and only 345 DEGs reached significance when the thresholds were relaxed ($p < 0.05$ and $|logFC| > 0.5$). AG-120 induced robust gene expression changes (1,513 DEGs at the relaxed threshold) but had only a minor impact on promoter methylation (47 out of 13,549 hypomethylated and 23

Figure 6. Synergistic activity of AG-120 and azacitidine

(A–C) I1DN tumor-bearing mice were treated with AG-120, azacitidine, the combination, or vehicle for 10 days and the disease burden in the bone marrow quantified by flow cytometry. The indicated progenitor (A and B) and mature (C) cell numbers are shown (n = 6 mice/group; data represented as mean ± SD; for A and C, p values were calculated using one-tailed, unpaired, non-parametric t test).

(D) Kaplan-Meier survival curve of I1DN tumor-bearing mice treated with AG-120, azacitidine, the combination, or vehicle. Gray shading denotes treatment (n = 6 mice/group; p value was calculated by log rank test).

(E) Bone marrow tumor burden (hCD45$^+$ cells as percentage of all viable cells) in the mIDH1 AML PDX model treated with AG-120, azacitidine, the combination, or vehicle. Mice were culled at pre-defined time points post enrollment (n = 4–10 mice/group; data represented as mean ± SD).

(F–I) RNA-seq and RRBS on cKit+ I1DN cells harvested from the bone marrow of I1DN engrafted mice treated for 5 days. (F) Heatmap of significantly methylated promoters (FDR < 0.05) in any drug condition relative to vehicle. (G) Volcano plots of DEGs ($p < 0.05$ and $|logFC| > 0.5$). (H) DEGs induced by the combination of AG-120 + azacitidine enhance the effect of AG-120. Violin plots demonstrating that DEGs induced by AG-120 + azacitidine are trending in the same direction as the single agents. p values were calculated using Student's t test. (I) Heatmap of genes from various GSEA pathways that are significant in AG-120 + azacitidine. *p < 0.05, **p < 0.01, ***p < 0.001, ****p < 0.0001.

out of 13,549 hypermethylated promoters), suggesting that acute transcriptional perturbation following IDH inhibition in I1DN promoters is not associated with demethylation of gene promoters (Figures 6F and 6G). Although a lower dose of AG-120 was used in this experiment compared with our earlier studies (150 mg/kg once daily versus 150 mg/kg twice a day), gene expression changes were highly concordant (Figure S6E). The combination of AG-120 and azacitidine had the greatest effects on both DNA methylation and gene expression. The majority of differentially methylated promoters were hypomethylated as expected (190 out of 13,549 hypomethylated and 58 out of 13,549 hypermethylated promoters) (Figure 6F). Interestingly, dual inhibition of mutant IDH1 and DNMT1 amplified the magnitude of gene expression changes induced by IDH1 inhibition alone (Figures 6H, 6I, and S6F). For example, genes that promote myeloid differentiation were further upregulated, while genes that underpin HSC function were further repressed by the combination (Figure 6I). Altogether, our data demonstrate that the AG-120 and azacitidine combination has superior efficacy to either agent alone in aggressive murine and human AML models and is potentially curative in some contexts.

DISCUSSION

Allosteric inhibitors of mutant IDH1/2 hold significant promise for the treatment of AML; however, resistance to single-agent therapy develops in almost all patients (Choe et al., 2020). Hence, there is a need to better understand mechanisms that dictate drug response and identify novel combination regimens. While data from clinical trials are accruing, studies in faithful model systems can provide valuable molecular insights that ultimately contribute to optimal drug deployment.

We developed a novel model of IDH1-mutant AML with co-expression of dominant-negative DNMT3A and oncogenic NRAS alleles. AML sequencing studies that have analyzed variant allele frequencies or mutational profiles at single-cell resolution have demonstrated that leukemic cells commonly carry three or more driver mutations (Miles et al., 2020; Papaemmanuil et al., 2016). Epigenetic mutations such as those in IDH1/2 and DNMT3A frequently co-occur in individual cells and are often present together in dominant leukemic clones, suggesting functional co-operation (Miles et al., 2020; Papaemmanuil et al., 2016). NRAS mutations are also common in IDH-mutant AML but are usually present in minor sub-clones at diagnosis (Miles et al., 2020; Papaemmanuil et al., 2016). The rapid outgrowth of cells expressing all three mutations in primary transplants in our study suggests that they jointly promote leukemia initiation. Our data are in agreement with earlier studies that investigated combinations of epigenetic and signaling mutations (Kats et al., 2017, 2014; Shih et al., 2017; Zhang et al., 2016).

The malignant hierarchies in AML differ significantly between patients, dictated by various genetic and cell-of-origin factors. In some cases, the majority of leukemic cells resemble early myeloid progenitors, whereas in others the bulk of the tumor is composed of more differentiated cell types (Miles et al., 2020; Quek et al., 2018; van Galen et al., 2019; Velten et al., 2021). Interestingly, NRAS mutations are associated with a late differentiation block and promote increased CD11b expression in IDH1-mutant AML clones (Miles et al., 2020). Consistent with these observations, we found that I1DN tumors were characterized by a differentiation block at the pre-neutrophil stage, with the majority of leukemic cells expressing CD11b. Thus, the I1DN model recapitulates epigenetic heterogeneity of human IDH/RAS double-mutant AML.

Mice bearing I1DN tumors responded to AG-120 single-agent treatment. Within 5 days of initiating therapy, we observed a shift in the leukemic progenitor compartment in the bone marrow to a more differentiated GMP-like immunophenotype. By 4 weeks, most of these cells were eliminated, leaving behind only a very small population of residual CMPs. This was accompanied by a progressive increase in differentiated myeloid cells. These observations are consistent with a model whereby IDH inhibitors target multiple levels of the AML hierarchy, limiting the self-renewal of LSCs as well as driving the differentiation of leukemic blasts, leading to disease exhaustion. Our findings underscore the complexity of accurately assessing therapeutic response in the clinical context. Most patients require several months of treatment to achieve their best morphologic response (Amatangelo et al., 2017; DiNardo et al., 2018), likely explained by the time required for LSCs to transit through the blast phase.

The molecular and cellular effects of AG-120 were highly similar to dox-induced genetic depletion of mutant IDH1, formally confirming the on-target activity of the inhibitor. GATA1 was upregulated by AG-120 and implicated as one of the key drivers of the transcriptional response in I1DN progenitors. Mutations in differentiation-associated transcription factors are associated with *de novo* and acquired resistance to IDH inhibitors in patients, suggesting a functional requirement for these pathways in the therapeutic response (Choe et al., 2020; Quek et al., 2018). Mutations in signaling pathways including NRAS are also associated with inferior response to IDH-targeting drugs and are often acquired or enriched at relapse (Choe et al., 2020; Quek et al., 2018). Our data demonstrate that NRAS mutations do not preclude response to single-agent IDH inhibition per se, although, concordant with clinical findings, AG-120 failed to completely eliminate the disease.

To explore the transcriptional heterogeneity of leukemic progenitors and its impact on drug response, we performed scRNA-seq. Recent single-cell lineage tracing studies in HSCs and AML have revealed that cells that are destined for long-term self-renewal or clonal dominance are characterized by an intrinsic and heritable gene expression profile (Fennell et al., 2021; Rodriguez-Fraticelli et al., 2020). Using established signatures from mice and humans, we identified a sub-population of quiescent I1DN progenitors that likely represent functional LSCs. The effects of AG-120 on gene expression were distinct in different cell types, suggesting that the maturation status of a leukemic cell is a major factor in dictating its response to IDH inhibition.

An inability to eradicate cancer stem cells and minimal residual disease is a major limitation of many cancer therapies, including targeted agents. The cells that survive initial treatment and ultimately serve as the reservoir for relapse typically represent a minor proportion of the initial tumor and are invisible to methods that analyze bulk cell populations. We found that AG-120 promoted cycling of LSCs and also increased expression of

pyrimidine salvage components in LSCs and other I1DN progenitors, leading us to test the combination of AG-120 with azacitidine. This proved to be highly effective in I1DN AML and in an IDH1-mutant PDX model. Consistent with our hypothesis that AG-120 promotes uptake of azacitidine in immature leukemic cells, the combination treatment caused loss of DNA methylation at gene promoters at a time when single-agent treatments had minimal impact on DNA methylation. Although we did not investigate the molecular mechanism by which AG-120 transcriptionally upregulates the pyrimidine salvage pathway in detail, analysis of gene expression during normal blood development suggests that it may be a consequence of myeloid differentiation induced by IDH inhibition.

Other recent studies in pre-clinical models have similarly reported synergy between IDH inhibitors and azacitidine (Chaturvedi et al., 2021; MacBeth et al., 2021) or between an IDH inhibitor, cytarabine (a cytosine analogue), and doxorubicin (Gupta et al., 2020). Chaturvedi et al. found that the combination of the IDH1 inhibitor BAY1436032 and azacitidine targets LSCs, and both Chaturvedi et al. and Gupta et al. observed that concurrent delivery of BAY1436032 and the cytosine analogue partner drug demonstrated superior anti-tumor activity compared with sequential dosing. These findings are concordant with our conclusion that the burst of differentiation and transcriptional changes that occur within days of IDH inhibitor treatment provide a potential window of opportunity for compounds that are more effective against rapidly proliferating cells. Most importantly, the increased benefit of the AG-120 and azacitidine combination has been observed in AML patients, including in a randomized multicenter phase 3 trial that reported a median overall survival of 24 months for the combination arm compared with 7.9 months in the azacitidine with placebo arm (DiNardo et al., 2021; Montesinos et al., 2022). The combination also appears to be more effective against tumors that carry mutations in kinase signaling pathway genes, with the majority of patients in this category achieving complete remission.

Together, our findings highlight the importance of understanding and analyzing the impact of epigenetic heterogeneity on drug response. A rapidly growing body of evidence suggests non-genetic mechanisms are a major component of drug resistance in cancer (Lewis and Kats, 2021; Marine et al., 2020). Developing rational strategies that can eliminate cells that have the potential to drive relapse will improve patient outcomes.

Limitations of the study

The I1DN mouse model was designed to delineate the role of mutant IDH1 in leukemia maintenance. While the model also includes two other AML oncogenes, DNMT3A^{R882H} and NRAS^{G12D}, we did not specifically examine the individual functions of those genes. We also did not directly investigate whether the molecular and cellular effects of IDH1 inhibition are altered in the presence of different co-occurring mutations. The I1DN model was generated by overexpression of mutant genes in fetal liver-derived HSPCs. Conversely, IDH and DNMT3A mutations predominantly occur in adult AML. Inappropriate timing or expression levels of the driving oncogenes from retroviral promoters and differences in the chromatin state of fetal and adult HSPCs potentially introduce artifacts into the I1DN model. However, our finding that AG-120 and azacitidine have combinatorial anti-tumor activity is supported by data in an independent PDX model and other published studies in model systems and patients as detailed above (Chaturvedi et al., 2021; DiNardo et al., 2021; Gupta et al., 2020; MacBeth et al., 2021; Montesinos et al., 2022).

STAR★METHODS

Detailed methods are provided in the online version of this paper and include the following:

- KEY RESOURCES TABLE
- RESOURCE AVAILABILITY
  - Lead contact
  - Data and code availability
- EXPERIMENTAL MODEL AND SUBJECT DETAILS
- METHOD DETAILS
  - Retroviral constructs
  - Retroviral generation and transduction of murine fetal liver cells
  - Transplantation and disease monitoring for the I1DN model
  - Limiting dilution transplant assay
  - I1DN therapy experiments
  - PDX therapy experiments
  - AG-120 and 2-HG measurements in mouse serum
  - Flow cytometry analysis and cell sorting
  - Western blot
  - RNA sequencing and analysis
  - RRBS sequencing and analysis
  - Exome sequencing and analysis
  - Single-cell RNA sequencing and analysis
- QUANTIFICATION AND STATISTICAL ANALYSIS

SUPPLEMENTAL INFORMATION

Supplemental information can be found online at https://doi.org/10.1016/j.celrep.2022.111182.

ACKNOWLEDGMENTS

We thank members of the molecular genomics, animal, and flow cytometry core facilities at the Peter MacCallum Cancer Centre for technical support; Brian Liddicoat for assistance with bisulfite sequencing; and Dylan Marchione and Emma Dion for critical review of the manuscript. This work was supported by a research grant from the National Health and Medical Research Council of Australia (APP1099160). The following authors were supported by fellowships: L.M.K. from the Victorian Cancer Agency (MCRF15003), A.C.L. from the Brazis family, J.S. from the Medical Research Future Fund of Australia (GNT1160133), and L.G.M. from The Lorenzo and Pamela Galli Medical Research Trust. E.G. was supported by the Australian Postgraduate Award.

AUTHOR CONTRIBUTIONS

Conceptualization and design, E.G., R.W.J., and L.M.K.; experiments and data analysis, E.G., J.S., A.C.L., R.F., R.C., L.G.M., A.J.R., E.V., P.F., K.S., L.J., A.T., N.T., J.L., and L.M.K.; technical expertise and essential reagents, B.N., S.D., A.T., and M.H.; supervision, J.S., R.W.J., and L.M.K.; writing and editing, E.G., R.W.J., and L.M.K.

DECLARATION OF INTERESTS

L.M.K. has received research funding and/or consultancy payments from Agios Pharmaceuticals, Celgene Corporation, and Servier Pharmaceuticals. J.S. has received research funding from BMS/Celgene, Amgen, and Astex Pharmaceuticals Inc., and served on the advisory boards of Astellas, Novartis, Otsuka, and Mundipharma. B.N., S.D., A.E.T., and M.L.H. were Agios employees, and S.D., A.E.T., and M.L.H. are, or were, Servier employees at the time of conducting these studies.

Received: March 7, 2022
Revised: June 9, 2022
Accepted: July 19, 2022
Published: August 16, 2022

REFERENCES

Aibar, S., González-Blas, C.B., Moerman, T., Huynh-Thu, V.A., Imrichova, H., Hulselmans, G., Rambow, F., Marine, J.-C., Geurts, P., Aerts, J., et al. (2017). SCENIC: single-cell regulatory network inference and clustering. Nat. Methods *14*, 1083–1086. https://doi.org/10.1038/nmeth.4463.

Akalin, A., Garrett-Bakelman, F.E., Kormaksson, M., Busuttil, J., Zhang, L., Khrebtukova, I., Milne, T.A., Huang, Y., Biswas, D., Hess, J.L., et al. (2012). Base-pair resolution DNA methylation sequencing reveals profoundly divergent epigenetic landscapes in acute myeloid leukemia. PLoS Genet. *8*, e1002781. https://doi.org/10.1371/journal.pgen.1002781.

Amatangelo, M.D., Quek, L., Shih, A., Stein, E.M., Roshal, M., David, M.D., Marteyn, B., Farnoud, N.R., de Botton, S., Bernard, O.A., et al. (2017). Enasidenib induces acute myeloid leukemia cell differentiation to promote clinical response. Blood *130*, 732–741. https://doi.org/10.1182/blood-2017-04-779447.

Bonnet, D., and Dick, J.E. (1997). Human acute myeloid leukemia is organized as a hierarchy that originates from a primitive hematopoietic cell. Nat. Med. *3*, 730–737. https://doi.org/10.1038/nm0797-730.

Butler, A., Hoffman, P., Smibert, P., Papalexi, E., and Satija, R. (2018). Integrating single-cell transcriptomic data across different conditions, technologies, and species. Nat. Biotechnol. *36*, 411–420. https://doi.org/10.1038/nbt.4096.

Cancer Genome Atlas Research Network; Ley, T.J., Miller, C., Ding, L., Raphael, B.J., Mungall, A.J., Robertson, A.G., Hoadley, K., Triche, T.J., Laird, P.W., Baty, J.D., et al. (2013). Genomic and epigenomic landscapes of adult de novo acute myeloid leukemia. N. Engl. J. Med. *368*, 2059–2074. https://doi.org/10.1056/NEJMoa1301689.

Chaturvedi, A., Gupta, C., Gabdoulline, R., Borchert, N.M., Goparaju, R., Kaulfuss, S., Görlich, K., Schottmann, R., Othman, B., Welzenbach, J., et al. (2021). Synergistic activity of IDH1 inhibitor BAY1436032 with azacitidine in IDH1 mutant acute myeloid leukemia. Haematologica *106*, 565–573.

Chen, C., Liu, Y., Lu, C., Cross, J.R., Morris, J.P., Shroff, A.S., Ward, P.S., Bradner, J.E., Thompson, C., and Lowe, S.W. (2013). Cancer-associated IDH2 mutants drive an acute myeloid leukemia that is susceptible to Brd4 inhibition. Genes Dev. *27*, 1974–1985. https://doi.org/10.1101/gad.226613.113.

Chen, Y., Pal, B., Visvader, J.E., and Smyth, G.K. (2017). Differential methylation analysis of reduced representation bisulfite sequencing experiments using edgeR. F1000Res. *6*, 2055. https://doi.org/10.12688/f1000research.13196.2.

Choe, S., Wang, H., DiNardo, C.D., Stein, E.M., de Botton, S., Roboz, G.J., Altman, J.K., Mims, A.S., Watts, J.M., Pollyea, D.A., et al. (2020). Molecular mechanisms mediating relapse following ivosidenib monotherapy in IDH1-mutant relapsed or refractory AML. Blood Adv. *4*, 1894–1905. https://doi.org/10.1182/bloodadvances.2020001503.

Cibulskis, K., Lawrence, M.S., Carter, S.L., Sivachenko, A., Jaffe, D., Sougnez, C., Gabriel, S., Meyerson, M., Lander, E.S., and Getz, G. (2013). Sensitive detection of somatic point mutations in impure and heterogeneous cancer samples. Nat. Biotechnol. *31*, 213–219. https://doi.org/10.1038/nbt.2514.

Danecek, P., Bonfield, J.K., Liddle, J., Marshall, J., Ohan, V., Pollard, M.O., Whitwham, A., Keane, T., McCarthy, S.A., Davies, R.M., and Li, H. (2021). Twelve years of SAMtools and BCFtools. Gigascience *10*, giab008. https://doi.org/10.1093/gigascience/giab008.

Dang, L., White, D.W., Gross, S., Bennett, B.D., Bittinger, M.A., Driggers, E.M., Fantin, V.R., Jang, H.G., Jin, S., Keenan, M.C., et al. (2009). Cancer-associated IDH1 mutations produce 2-hydroxyglutarate. Nature *462*, 739–744. https://doi.org/10.1038/nature08617.

DiNardo, C.D., Stein, E.M., de Botton, S., Roboz, G.J., Altman, J.K., Mims, A.S., Swords, R., Collins, R.H., Mannis, G.N., Pollyea, D.A., et al. (2018). Durable remissions with ivosidenib in IDH1-mutated relapsed or refractory AML. N. Engl. J. Med. *378*, 2386–2398. https://doi.org/10.1056/NEJMoa1716984.

DiNardo, C.D., Stein, A.S., Stein, E.M., Fathi, A.T., Frankfurt, O., Schuh, A.C., Döhner, H., Martinelli, G., Patel, P.A., Raffoux, E., et al. (2021). Mutant isocitrate dehydrogenase 1 inhibitor ivosidenib in combination with azacitidine for newly diagnosed acute myeloid leukemia. J. Clin. Oncol. *39*, 57–65. https://doi.org/10.1200/JCO.20.01632.

Evrard, M., Kwok, I.W.H., Chong, S.Z., Teng, K.W.W., Becht, E., Chen, J., Sieow, J.L., Penny, H.L., Ching, G.C., Devi, S., et al. (2018). Developmental analysis of bone marrow neutrophils reveals populations specialized in expansion, trafficking, and effector functions. Immunity *48*, 364–378.e9. https://doi.org/10.1016/j.immuni.2018.02.002.

Fennell, K.A., Vassiliadis, D., Lam, E.Y.N., Martelotto, L.G., Balic, J.J., Hollizeck, S., Weber, T.S., Semple, T., Wang, Q., Miles, D.C., et al. (2021). Nongenetic determinants of malignant clonal fitness at single-cell resolution. Nature *601*, 125–131. https://doi.org/10.1038/s41586-021-04206-7.

Figueroa, M.E., Abdel-Wahab, O., Lu, C., Ward, P.S., Patel, J., Shih, A., Li, Y., Bhagwat, N., Vasanthakumar, A., Fernandez, H.F., et al. (2010). Leukemic IDH1 and IDH2 mutations result in a hypermethylation phenotype, disrupt TET2 function, and impair hematopoietic differentiation. Cancer Cell *18*, 553–567. https://doi.org/10.1016/j.ccr.2010.11.015.

Fong, C.Y., Gilan, O., Lam, E.Y.N., Rubin, A.F., Ftouni, S., Tyler, D., Stanley, K., Sinha, D., Yeh, P., Morison, J., et al. (2015). BET inhibitor resistance emerges from leukaemia stem cells. Nature *525*, 538–542. https://doi.org/10.1038/nature14888.

Gruber, E., Franich, R.L., Shortt, J., Johnstone, R.W., and Kats, L.M. (2020). Distinct and overlapping mechanisms of resistance to azacytidine and guadecitabine in acute myeloid leukemia. Leukemia *34*, 3388–3392. https://doi.org/10.1038/s41375-020-0973-z.

Gu, X., Tohme, R., Tomlinson, B., Sakre, N., Hasipek, M., Durkin, L., Schuerger, C., Grabowski, D., Zidan, A.M., Radivoyevitch, T., et al. (2020). Decitabine- and 5-azacytidine resistance emerges from adaptive responses of the pyrimidine metabolism network. Leukemia *35*, 1023–1036. https://doi.org/10.1038/s41375-020-1003-x.

Gupta, C., Kaulfuss, S., Gorlich, K., Othman, B., Chaturvedi, A., and Heuser, M. (2020). Combination treatment of an IDH1 inhibitor with chemotherapy in IDH1 mutant acute myeloid leukemia. Ann. Hematol. *99*, 1415–1417.

Hamey, F.K., and Göttgens, B. (2019). Machine learning predicts putative hematopoietic stem cells within large single-cell transcriptomics data sets. Exp. Hematol. *78*, 11–20. https://doi.org/10.1016/j.exphem.2019.08.009.

Harding, J.J., Lowery, M.A., Shih, A.H., Schvartzman, J.M., Hou, S., Famulare, C., Patel, M., Roshal, M., Do, R.K., Zehir, A., et al. (2018). Isoform switching as a mechanism of acquired resistance to mutant isocitrate dehydrogenase inhibition. Cancer Discov. *8*, 1540–1547. https://doi.org/10.1158/2159-8290.CD-18-0877.

Hoppe, P.S., Schwarzfischer, M., Loeffler, D., Kokkaliaris, K.D., Hilsenbeck, O., Moritz, N., Endele, M., Filipczyk, A., Gambardella, A., Ahmed, N., et al. (2016). Early myeloid lineage choice is not initiated by random PU.1 to GATA1 protein ratios. Nature *535*, 299–302. https://doi.org/10.1038/nature18320.

Intlekofer, A.M., Shih, A.H., Wang, B., Nazir, A., Rustenburg, A.S., Albanese, S.K., Patel, M., Famulare, C., Correa, F.M., Takemoto, N., et al. (2018). Acquired resistance to IDH inhibition through trans or cis dimer-interface mutations. Nature *559*, 125–129. https://doi.org/10.1038/s41586-018-0251-7.

Juarez, J.G., Harun, N., Thien, M., Welschinger, R., Baraz, R., Pena, A.D., Pitson, S.M., Rettig, M., DiPersio, J.F., Bradstock, K.F., and Bendall, L.J. (2012). Sphingosine-1-phosphate facilitates trafficking of hematopoietic stem cells and their mobilization by CXCR4 antagonists in mice. Blood *119*, 707–716. https://doi.org/10.1182/blood-2011-04-348904.

Kats, L.M., Reschke, M., Taulli, R., Pozdnyakova, O., Burgess, K., Bhargava, P., Straley, K., Karnik, R., Meissner, A., Small, D., et al. (2014). Proto-oncogenic role of mutant IDH2 in leukemia initiation and maintenance. Cell Stem Cell *14*, 329–341. https://doi.org/10.1016/j.stem.2013.12.016.

Kats, L.M., Vervoort, S.J., Cole, R., Rogers, A.J., Gregory, G.P., Vidacs, E., Li, J., Nagaraja, R., Yen, K.E., and Johnstone, R.W. (2017). A pharmacogenomic approach validates AG-221 as an effective and on-target therapy in IDH2 mutant AML. Leukemia *31*, 1466–1470. https://doi.org/10.1038/leu.2017.84.

Kim, D., Langmead, B., and Salzberg, S.L. (2015). HISAT: a fast spliced aligner with low memory requirements. Nat. Methods *12*, 357–360. https://doi.org/10.1038/nmeth.3317.

Koivunen, P., Lee, S., Duncan, C.G., Lopez, G., Lu, G., Ramkissoon, S., Losman, J.A., Joensuu, P., Bergmann, U., Gross, S., et al. (2012). Transformation by the (R)-enantiomer of 2-hydroxyglutarate linked to EGLN activation. Nature *483*, 484–488. https://doi.org/10.1038/nature10898.

Korotkevich, G., Sukhov, V., Budin, N., Shpak, B., Artyomov, M.N., and Sergushichev, A. (2021). Fast gene set enrichment analysis. Preprint at bioRxiv. https://doi.org/10.1101/060012.

Krueger, F., and Andrews, S.R. (2011). Bismark: a flexible aligner and methylation caller for Bisulfite-Seq applications. Bioinformatics *27*, 1571–1572. https://doi.org/10.1093/bioinformatics/btr167.

Lane, A.N., and Fan, T.W.M. (2015). Regulation of mammalian nucleotide metabolism and biosynthesis. Nucleic Acids Res. *43*, 2466–2485. https://doi.org/10.1093/nar/gkv047.

Lara-Astiaso, D., Weiner, A., Lorenzo-Vivas, E., Zaretsky, I., Jaitin, D.A., David, E., KerenShaul, H., Mildner, A., Winter, D., Jung, S., et al. (2014). Immunogenetics. Chromatin state dynamics during blood formation. Science *345*, 943–949. https://doi.org/10.1126/science.1256271.

Lechman, E.R., Gentner, B., Ng, S.W.K., Schoof, E.M., van Galen, P., Kennedy, J.A., Nucera, S., Ciceri, F., Kaufmann, K.B., Takayama, N., et al. (2016). miR-126 regulates distinct self-renewal outcomes in normal and malignant hematopoietic stem cells. Cancer Cell *29*, 214–228. https://doi.org/10.1016/j.ccell.2015.12.011.

Lai, Z., Markovets, A., Ahdesmaki, M., Chapman, B., Hofmann, O., McEwen, R., Johnson, J., Dougherty, B., Barrett, J.C., and Dry, J.R. (2016). VarDict: a novel and versatile variant caller for next-generation sequencing in cancer research. Nucleic Acids Res. *44*, e108. https://doi.org/10.1093/nar/gkw227.

Lewis, A.C., and Kats, L.M. (2021). Non-genetic heterogeneity, altered cell fate and differentiation therapy. EMBO Mol. Med. *13*, e12670. https://doi.org/10.15252/emmm.202012670.

Li, H. (2011). Tabix: fast retrieval of sequence features from generic TAB-delimited files. Bioinformatics *27*, 718–719. https://doi.org/10.1093/bioinformatics/btq671.

Li, H. (2013). Aligning sequence reads, clone sequences and assembly contigs with BWA-MEM. Preprint at arXiv.

Li, H., Handsaker, B., Wysoker, A., Fennell, T., Ruan, J., Homer, N., Marth, G., Abecasis, G., and Durbin, R.; 1000 Genome Project Data Processing Subgroup (2009). The sequence alignment/map format and SAMtools. Bioinformatics *25*, 2078–2079. https://doi.org/10.1093/bioinformatics/btp352.

Liao, Y., Smyth, G.K., and Shi, W. (2014). featureCounts: an efficient general purpose program for assigning sequence reads to genomic features. Bioinformatics *30*, 923–930. https://doi.org/10.1093/bioinformatics/btt656.

Losman, J.-A., Looper, R.E., Koivunen, P., Lee, S., Schneider, R.K., McMahon, C., Cowley, G.S., Root, D.E., Ebert, B.L., and Kaelin, W.G. (2013). (R)-2-hydroxyglutarate is sufficient to promote leukemogenesis and its effects are reversible. Science *339*, 1621–1625. https://doi.org/10.1126/science.1231677.

Lu, C., Ward, P.S., Kapoor, G.S., Rohle, D., Turcan, S., Abdel-Wahab, O., Edwards, C.R., Khanin, R., Figueroa, M.E., Melnick, A., et al. (2012). IDH mutation impairs histone demethylation and results in a block to cell differentiation. Nature *483*, 474–478. https://doi.org/10.1038/nature10860.

MacBeth, K.J., Chopra, V.S., Tang, L., Zheng, B., Avanzino, B., See, W.L., Schwickart, M., Figueroa, M.E., Quek, L., and DiMartino, J.F. (2021). Combination of azacitidine and enasidenib enhances leukemic cell differentiation and cooperatively hypomethylates DNA. Exp. Hematol. https://doi.org/10.1016/j.exphem.2021.03.003.

Mardis, E.R., Ding, L., Dooling, D.J., Larson, D.E., McLellan, M.D., Chen, K., Koboldt, D.C., Fulton, R.S., Delehaunty, K.D., McGrath, S.D., et al. (2009). Recurring mutations found by sequencing an acute myeloid leukemia genome. N. Engl. J. Med. *361*, 1058–1066. https://doi.org/10.1056/NEJMoa0903840.

Marine, J.-C., Dawson, S.-J., and Dawson, M.A. (2020). Non-genetic mechanisms of therapeutic resistance in cancer. Nat. Rev. Cancer *20*, 743–756. https://doi.org/10.1038/s41568-020-00302-4.

Martin, M. (2011). Cutadapt removes adapter sequences from high-throughput sequencing reads. EMBnet.J. *17*, 10–12. https://doi.org/10.14806/ej.17.1.200.

McBrayer, S.K., Mayers, J.R., DiNatale, G.J., Shi, D.D., Khanal, J., Chakraborty, A.A., Sarosiek, K.A., Briggs, K.J., Robbins, A.K., Sewastianik, T., et al. (2018). Transaminase inhibition by 2-hydroxyglutarate impairs glutamate biosynthesis and redox homeostasis in glioma. Cell *175*, 101–116.e25. https://doi.org/10.1016/j.cell.2018.08.038.

McCarthy, D.J., Chen, Y., and Smyth, G.K. (2012). Differential expression analysis of multifactor RNA-Seq experiments with respect to biological variation. Nucleic Acids Res. *40*, 4288–4297. https://doi.org/10.1093/nar/gks042.

McLaren, W., Gil, L., Hunt, S.E., Riat, H.S., Ritchie, G.R.S., Thormann, A., Flicek, P., and Cunningham, F. (2016). The ensembl variant effect predictor. Genome Biol. *17*, 122. https://doi.org/10.1186/s13059-016-0974-4.

Miles, L.A., Bowman, R.L., Merlinsky, T.R., Csete, I.S., Ooi, A.T., Durruthy-Durruthy, R., Bowman, M., Famulare, C., Patel, M.A., Mendez, P., et al. (2020). Single-cell mutation analysis of clonal evolution in myeloid malignancies. Nature *587*, 477–482. https://doi.org/10.1038/s41586-020-2864-x.

Montesinos, P., Recher, C., Vives, S., Zarzycka, E., Wang, J., Bertani, G., Heuser, M., Calado, R.T., Schuh, A.C., Yeh, S.P., et al. (2022). Ivosidenib and azacitidine in IDH1-mutated acute myeloid leukemia. N. Engl. J. Med. *386*, 1519–1531.

Morita, K., Wang, F., Jahn, K., Hu, T., Tanaka, T., Sasaki, Y., Kuipers, J., Loghavi, S., Wang, S.A., Yan, Y., et al. (2020). Clonal evolution of acute myeloid leukemia revealed by high-throughput single-cell genomics. Nat. Commun. *11*, 5327. https://doi.org/10.1038/s41467-020-19119-8.

Ng, S.W.K., Mitchell, A., Kennedy, J.A., Chen, W.C., McLeod, J., Ibrahimova, N., Arruda, A., Popescu, A., Gupta, V., Schimmer, A.D., et al. (2016). A 17-gene stemness score for rapid determination of risk in acute leukaemia. Nature *540*, 433–437. https://doi.org/10.1038/nature20598.

Papaemmanuil, E., Gerstung, M., Bullinger, L., Gaidzik, V.I., Paschka, P., Roberts, N.D., Potter, N.E., Heuser, M., Thol, F., Bolli, N., et al. (2016). Genomic classification and prognosis in acute myeloid leukemia. N. Engl. J. Med. *374*, 2209–2221. https://doi.org/10.1056/NEJMoa1516192.

Parsons, D.W., Jones, S., Zhang, X., Lin, J.C.H., Leary, R.J., Angenendt, P., Mankoo, P., Carter, H., Siu, I.-M., Gallia, G.L., et al. (2008). An integrated genomic analysis of human glioblastoma multiforme. Science *321*, 1807–1812. https://doi.org/10.1126/science.1164382.

Quek, L., David, M.D., Kennedy, A., Metzner, M., Amatangelo, M., Shih, A., Stoilova, B., Quivoron, C., Heiblig, M., Willekens, C., et al. (2018). Clonal heterogeneity of acute myeloid leukemia treated with the IDH2 inhibitor enasidenib. Nat. Med. *24*, 1167–1177. https://doi.org/10.1038/s41591-018-0115-6.

Quinlan, A.R., and Hall, I.M. (2010). BEDTools: a flexible suite of utilities for comparing genomic features. Bioinformatics *26*, 841–842. https://doi.org/10.1093/bioinformatics/btq033.

Rapin, N., Bagger, F.O., Jendholm, J., Mora-Jensen, H., Krogh, A., Kohlmann, A., Thiede, C., Borregaard, N., Bullinger, L., Winther, O., et al. (2014).

Comparing cancer vs normal gene expression profiles identifies new disease entities and common transcriptional programs in AML patients. Blood *123*, 894–904.

Ritchie, M.E., Phipson, B., Wu, D., Hu, Y., Law, C.W., Shi, W., and Smyth, G.K. (2015). limma powers differential expression analyses for RNA-sequencing and microarray studies. Nucleic Acids Res. *43*, e47. https://doi.org/10.1093/nar/gkv007.

Rodriguez-Fraticelli, A.E., Weinreb, C., Wang, S.-W., Migueles, R.P., Jankovic, M., Usart, M., Klein, A.M., Lowell, S., and Camargo, F.D. (2020). Single-cell lineage tracing unveils a role for TCF15 in haematopoiesis. Nature *583*, 585–589. https://doi.org/10.1038/s41586-020-25036.

Sasaki, M., Knobbe, C.B., Itsumi, M., Elia, A.J., Harris, I.S., Chio, I.I.C., Cairns, R.A., McCracken, S., Wakeham, A., Haight, J., et al. (2012a). D-2hydroxyglutarate produced by mutant IDH1 perturbs collagen maturation and basement membrane function. Genes Dev. *26*, 2038–2049. https://doi.org/10.1101/gad.198200.112.

Sasaki, M., Knobbe, C.B., Munger, J.C., Lind, E.F., Brenner, D., Brüstle, A., Harris, I.S., Holmes, R., Wakeham, A., Haight, J., et al. (2012b). IDH1(R132H) mutation increases murine haematopoietic progenitors and alters epigenetics. Nature *488*, 656–659. https://doi.org/10.1038/nature11323.

Shih, A.H., Meydan, C., Shank, K., Garrett-Bakelman, F.E., Ward, P.S., Intlekofer, A.M., Nazir, A., Stein, E.M., Knapp, K., Glass, J., et al. (2017). Combination targeted therapy to disrupt aberrant oncogenic signaling and reverse epigenetic dysfunction in IDH2- and TET2-mutant acute myeloid leukemia. Cancer Discov. *7*, 494–505. https://doi.org/10.1158/2159-8290.CD-16-1049.

Stein, E.M., DiNardo, C.D., Pollyea, D.A., Fathi, A.T., Roboz, G.J., Altman, J.K., Stone, R.M., DeAngelo, D.J., Levine, R.L., Flinn, I.W., et al. (2017). Enasidenib in mutant IDH2 relapsed or refractory acute myeloid leukemia. Blood *130*, 722–731. https://doi.org/10.1182/blood-2017-04-779405.

Subramanian, A., Tamayo, P., Mootha, V.K., Mukherjee, S., Ebert, B.L., Gillette, M.A., Paulovich, A., Pomeroy, S.L., Golub, T.R., Lander, E.S., and Mesirov, J.P. (2005). Gene set enrichment analysis: a knowledge-based approach for interpreting genome-wide expression profiles. Proc. Natl. Acad. Sci. USA. *102*, 15545–15550. https://doi.org/10.1073/pnas.0506580102.

Tirosh, I., Izar, B., Prakadan, S.M., Wadsworth, M.H., Treacy, D., Trombetta, J.J., Rotem, A., Rodman, C., Lian, C., Murphy, G., et al. (2016). Dissecting the multicellular ecosystem of metastatic melanoma by single-cell RNA-seq. Science *352*, 189–196. https://doi.org/10.1126/science.aad0501.

Unnikrishnan, A., Papaemmanuil, E., Beck, D., Deshpande, N.P., Verma, A., Kumari, A., Woll, P.S., Richards, L.A., Knezevic, K., Chandrakanthan, V., et al. (2017). Integrative genomics identifies the molecular basis of resistance to azacitidine therapy in myelodysplastic syndromes. Cell Rep. *20*, 572–585. https://doi.org/10.1016/j.celrep.2017.06.067.

Unnikrishnan, A., Vo, A.N.Q., Pickford, R., Raftery, M.J., Nunez, A.C., Verma, A., Hesson, L.B., and Pimanda, J.E. (2018). AZA-MS: a novel multiparameter mass spectrometry method to determine the intracellular dynamics of azacitidine therapy in vivo. Leukemia *32*, 900–910. https://doi.org/10.1038/leu.2017.340.

Van der Auwera, G.A., Carneiro, M.O., Hartl, C., Poplin, R., Del Angel, G., Levy-Moonshine, A., Jordan, T., Shakir, K., Roazen, D., Thibault, J., et al. (2013). From FastQ data to high confidence variant calls: the Genome Analysis Toolkit best practices pipeline. Curr. Protoc. Bioinformatics *43*, 11.10.1–11.10.33. https://doi.org/10.1002/0471250953.bi1110s43.

van Galen, P., Hovestadt, V., Wadsworth, M.H., II, Hughes, T.K., Griffin, G.K., Battaglia, S., Verga, J.A., Stephansky, J., Pastika, T.J., Story, J.L., et al. (2019). Single-cell RNA-seq reveals AML hierarchies relevant to disease progression and immunity. Cell *176*, 1265–1281.e24. https://doi.org/10.1016/j.cell.2019.01.031.

Velten, L., Story, B.A., Hernández-Malmierca, P., Raffel, S., Leonce, D.R., Milbank, J., Paulsen, M., Demir, A., Szu-Tu, C., Frömel, R., et al. (2021). Identification of leukemic and pre-leukemic stem cells by clonal tracking from single-cell transcriptomics. Nat. Commun. *12*, 1366. https://doi.org/10.1038/s41467-02121650-1.

Wang, G.G., Pasillas, M.P., and Kamps, M.P. (2005). Meis1 programs transcription of FLT3 and cancer stem cell character, using a mechanism that requires interaction with Pbx and a novel function of the Meis1 C-terminus. Blood *106*, 254–264. https://doi.org/10.1182/blood-200412-4664.

Wang, F., Morita, K., DiNardo, C.D., Furudate, K., Tanaka, T., Yan, Y., Patel, K.P., MacBeth, K.J., Wu, B., Liu, G., et al. (2021). Leukemia stemness and co-occurring mutations drive resistance to IDH inhibitors in acute myeloid leukemia. Nat. Commun. *12*, 2607–2613. https://doi.org/10.1038/s41467-021-22874-x.

Wu, D., Lim, E., Vaillant, F., Asselin-Labat, M.-L., Visvader, J.E., and Smyth, G.K. (2010). ROAST: rotation gene set tests for complex microarray experiments. Bioinformatics *26*, 2176–2182. https://doi.org/10.1093/bioinformatics/btq401.

Xu, W., Yang, H., Liu, Y., Yang, Y., Wang, P., Kim, S.-H., Ito, S., Yang, C., Wang, P., Xiao, M.-T., et al. (2011). Oncometabolite 2hydroxyglutarate is a competitive inhibitor of α-ketoglutarate-dependent dioxygenases. Cancer Cell *19*, 17–30. https://doi.org/10.1016/j.ccr.2010.12.014.

Yu, G., Wang, L.-G., Han, Y., and He, Q.-Y. (2012). clusterProfiler: an R package for comparing biological themes among gene clusters. OMICS *16*, 284–287. https://doi.org/10.1089/omi.2011.0118.

Zhang, H., Alberich-Jorda, M., Amabile, G., Yang, H., Staber, P.B., Di Ruscio, A., Welner, R.S., Ebralidze, A., Zhang, J., Levantini, E., et al. (2013). Sox4 is a key oncogenic target in C/EBPα mutant acute myeloid leukemia. Cancer Cell *24*, 575–588. https://doi.org/10.1016/j.ccr.2013.09.018.

Zhang, X., Su, J., Jeong, M., Ko, M., Huang, Y., Park, H.J., Guzman, A., Lei, Y., Huang, Y.H., Rao, A., et al. (2016). DNMT3A and TET2 compete and cooperate to repress lineage-specific transcription factors in hematopoietic stem cells. Nat. Genet. *48*, 1014–1023. https://doi.org/10.1038/ng.3610.

STAR★METHODS

KEY RESOURCES TABLE

REAGENT or RESOURCE	SOURCE	IDENTIFIER
Antibodies		
Anti-Mouse IgG/HRP	Dako	Cat# P0260; RRID: AB_2636929
Anti-Rabbit IgG/HRP	Dako	Cat# P0217; RRID: AB_2728719
B220 APC-E780	Invitrogen	Cat# 47-0452-82
β-actin	Sigma	Cat# A2228; RRID: AB_476697
CD11b APC-E780	Thermo Fisher	Cat# 47-0112-82; RRID: AB_1603193
CD11b Biotin	MACS Miltenyi Biotech	Cat# 130-113-233; RRID: AB_2726044
CD11b BV450	BD Horizon	Cat# 560455
CD11b BV711	Biolegend	Cat# 560455
CD16/CD32 (FCγR-III) BV786	BD Optibuild	Cat# 740851
CD16/CD32 (FCγR-III) BUV737	BD Horizon	Cat# 565272
CD34 BV421	BD Biosciences	Cat# 562608
CD115 Superbright436	Invitrogen	Cat# 62-1152-82
CD117 APC	BD Pharmingen	Cat# 553356; RRID: AB_398536
CD117 BV650	BD Horizon	Cat# 563553
CD182 APC	Biolegend	Cat# 149312; RRID: AB_2728185
CD184 BUV395	BD Optibuild	Cat# 740265; RRID: AB_2740007
DNMT3A	Cell Signaling	Cat# 2160s; RRID: AB_2263617
IDH1	Cell Signaling	Cat# 8137s; RRID: AB_10950504
Ly-6A/E (Sca1) Pe/Cy7	BD Pharmingen	Cat# 558162; RRID: AB_647253
Ly-6C BV421	Biolegend	Cat# 128032; RRID: AB_2562178
Ly-6C BV785	Biolegend	Cat# 128041
Ly-6G BV605	Biolgened	Cat# 127639; RRID: AB_2565880
NK1.1 APC/Cy7	BD Pharmingen	Cat# 560618; RRID: AB_1727569
$NRAS^{G12D}$	Cell Signaling	Cat# 14429s; RRID: AB_2728748
Siglec-F BV421	BD Horizon	Cat# 562681; RRID: AB_2722581
Siglec-F BV786	BD Optibuild	Cat# 740956
Streptavidin APC/Cy7	Biolegend	Cat# 405208
TCRβ APC-E780	eBioscience	Cat# 47-5961-82; RRID: AB_1272173
TCRβ E450	eBioscience	Cat# 48-5961-82
Bacterial and virus strains		
pCL-Eco	Addgene	Cat# 12371
Chemicals, peptides, and recombinant proteins		
5-Azacytidine	Sigma	Cat# A2385
AG-120 SDD	Agios Pharmaceuticals	N/A
HPMCAS	Agios Pharmaceuticals	N/A
TRIzol Reagent	Invitrogen	Cat# 15596018
Critical commercial assays		
Chromium Single Cell 5′ Library & Gel Bead Kit	10X genomics	PN-1000006
Direct-zol RNA Microprep kit	Zymo Research	Cat# R2062
Premium RRBS kit	Diagenode	Cat# C02030033
QuantSeq 3′ mRNA-seq Library Prep Kit for Illumina	Lexogen	Cat# 015

(*Continued on next page*)

Continued

REAGENT or RESOURCE	SOURCE	IDENTIFIER
Quick-DNA Microprep Kit	Zymo Research	Cat# D3020
Deposited data		
RNA-sequencing of I1DN progenitor (cKit+CD11b-) cells from mice treated with vehicle or AG-120 for 5 or 14 days, or treated with AG-120 for the full 28 days and relapsed after treatment.	This paper	GEO: GSE201662
Single-cell RNA-sequencing of I1DN progenitor (cKit+CD11b-) cells from mice treated with vehicle or AG-120 for 5 days.	This paper	GEO: GSE201664
RNA-sequencing of I1DN progenitor (cKit+CD11b-) cells from mice treated with vehicle, AG-120, AZA, or the combination of AG-120 and AZA for 5 days.	This paper	GEO: GSE201661
Reduced representation bisulfite sequencing of I1DN progenitor (cKit+CD11b-) cells from mice treated with vehicle, AG-120, AZA, or the combination of AG-120 and AZA for 5 days.	This paper	GEO: GSE201663
Experimental models: Organisms/strains		
Mouse: C57BL/6	Walter and Eliza Hall Institute of Medical Research	N/A
Mouse: C57BL/6.SJL-Ptprca	Walter and Eliza Hall Institute of Medical Research	N/A
Mouse: NOD.Cg-Prkdcscid Il2rgtm1Wjl/SzJ	Peter MacCallum Cancer Center	N/A
Recombinant DNA		
Plasmid: MSCV-TREtight-dsRED-IRES-IDH1^{R132H}	This paper	N/A
Plasmid: MSCV-Nras^{G12D}-IRES-tTA	Gift from Johannes Zuber (Research Institute of Molecular Pathology, Vienna, Austria)	N/A
Plasmid: MSCV-DNMT3A^{R82H}-IRES-GFP	Gift from Yueying Wang (Shanghai Institute of Hematology, Shanghai, China)	N/A
Software and algorithms		
BCFtools (v 1.3.1)	(Danecek et al., 2021)	https://samtools.github.io/bcftools/bcftools.html
bcl2fastq (v 2.17.1.14)	Illumina	https://sapac.support.illumina.com/
BEDTools (v 2.21.0)	(Quinlan and Hall, 2010)	https://github.com/arq5x/bedtools2
Bismark (v 0.22.3)	(Krueger and Andrews, 2011)	https://www.bioinformatics.babraham.ac.uk/projects/bismark/
BWA-MEM	(Li, 2013)	https://github.com/lh3/bwa
Cell Ranger (v 3.1.0)	10X Genomics	https://support.10xgenomics.com/single-cell-gene-expression/software/downloads/latest
clusterProfiler (v 3.18.0)	(Yu et al., 2012)	https://github.com/YuLab-SMU/clusterProfiler
cutadapt (v 1.14)	(Martin, 2011)	https://cutadapt.readthedocs.io/en/stable/
EdgeR (v 3.28.1, 3.32.1)	(Chen et al., 2017; McCarthy et al., 2012)	https://bioconductor.org/packages/release/workflows/vignettes/RnaSeqGeneEdgeRQL/inst/doc/edgeRQL.html https://www.bioconductor.org/packages/release/bioc/vignettes/edgeR/inst/doc/edgeRUsersGuide.pdf

(*Continued on next page*)

Continued

REAGENT or RESOURCE	SOURCE	IDENTIFIER
fgsea (v 1.16.0)	(Korotkevich et al., 2021)	https://github.com/ctlab/fgsea
FlowJo (v 10.7.2)		https://www.flowjo.com/
GATK-Mutect2 (v 3.9.0)	(Van der Auwera et al., 2013)	https://gatk.broadinstitute.org/hc/en-us/articles/360037593851-Mutect2
ggplot2 (v 3.2.1, 3.3.3)	CRAN	https://cran.r-project.org/web/packages/ggplot2/index.html
GSEA	(Subramanian et al., 2005)	https://www.gsea-msigdb.org/gsea/index.jsp
HISAT2 (v 2.1.0)	(Kim et al., 2015)	http://daehwankimlab.github.io/hisat2/manual/
Limma (v 3.42.2)	(Ritchie et al., 2015)	https://bioinf.wehi.edu.au/limma/
MuTect (v 1.17)	(Cibulskis et al., 2013)	https://software.broadinstitute.org/cancer/cga/mutect
Prism (v 9.2.0)		https://www.graphpad.com/scientific-software/prism/
R (v 3.6, 4.0.2)	R Development Core Team, 2008	http://www.R-project.org
RCisTarget (v 1.11.10)	(Aibar et al., 2017)	https://github.com/aertslab/RcisTarget
Samtools (v 1.4.1)	(Li et al., 2009)	http://samtools.sourceforge.net/
Seurat (v 4.0.4)	(Butler et al., 2018)	https://satijalab.org/seurat/
Subread (v 1.6.3)	(Liao et al., 2014)	http://subread.sourceforge.net/
Tabix (v 0.2.5)	(Li, 2011)	http://www.htslib.org/doc/tabix.html
Vardict (v 1.4.6)	(Lai et al., 2016)	https://github.com/AstraZeneca-NGS/VarDict
Variant Effect Predictor (VEP) release 90	(McLaren et al., 2016)	https://github.com/Ensembl/ensembl-vep

RESOURCE AVAILABILITY

Lead contact

Further information and requests for resources and reagents should be directed to and will be fulfilled by the lead contact, Lev Kats (lev.lats@petermac.org).

Materials availability

This study did not generate new unique reagents.

Data and code availability

- Processed and unprocessed data for RNAseq, scRNAseq and RRBS has been deposited to GEO under the superseries accession number GEO: GSE201665.
- This data does not report original code.
- All other data is available from the corresponding author on request.

EXPERIMENTAL MODEL AND SUBJECT DETAILS

All animal experiments related to the I1DN mouse model were performed at the Peter MacCallum Cancer Center and were approved by the Peter MacCallum Cancer Center Animal Experimentation Ethics Committee. Wild-type C57BL/6, congenic C57BL/6.SJL-Ptprca (referred throughout the text as *Ptprca*) and immune deficient NOD.Cg-Prkdcscid Il2rgtm1Wjl/SzJ (referred to as NSG) mice were purchased from the Animal Resources Center of Peter MacCallum Cancer Center or the Walter and Eliza Hall Institute of Medical Research (Melbourne, Australia). All experimental mice were housed at the Peter MacCallum Cancer Center under specific pathogen-free conditions. Animals were group-housed in individually ventilated micro-isolator cages (6 mice per cage) on a 13-h light/11-h dark cycle. Mice had continuous access to sterilized water and Barastoc irradiated mouse cubes (Ridley AgriProducts). The patient derived xenograft study (PDX) was performed by Champions Oncology (NJ, USA) under approved protocol #1029-018 and commissioned by Agios Pharmaceuticals. NOD.Cg-Prkdcscid Il2rgtm1Sug/JicTac (NOG) female mice were supplied by Taconic and housed in individual HEPA ventilated cages on a 14 h light/10-h dark cycle.

METHOD DETAILS

Retroviral constructs

All retroviruses were based on an MSCV backbone (Clonetech). The doxycycline (doxy)-inducible construct TRI-IDHR132H was generated by replacing the open reading frame encoding MLL-AF9 with an open reading frame encoding the human IDH1R132H allele. MIT-NRASG12D and MIG-DNMT3AR882H were kind gifts from Johannes Zuber (Research Institute of Molecular Pathology, Vienna, Austria) and Yueying Wang (Shanghai Institute of Hematology, Shanghai, China), respectively.

Retroviral generation and transduction of murine fetal liver cells

HEK-293T cells, seeded at approximately 50% confluence 24 h prior to transfection, were transiently transfected using the calcium phosphate method. A solution of retroviral DNA plasmids (TRI-dsRED-IDH1^{R132H}, MSCV-GFP-DNMT3A^{R882H}, MSCV-tTA-Nras^{G12D}, pcl-Eco packaging vector (Addgene plasmid cat# 12371), 0.25 M $CaCl_2$, 1.25 mM HEPES buffered H_2O was added dropwise to an equivalent volume of 2x HEBS buffer (HEPES 50 mM, NaCl 180 mM, Na_2HPO_4 1.5 mM pH 7) whilst air was bubbled through. The transfection mixture was incubated at room temperature for 20 min then added dropwise to the HEK-293T cells. Embryonic day 13.5–14.5 fetal liver cells (FLCs) were harvested from C57BL/6 embryos and cultured overnight in Dulbecco's Modified Eagle Medium (DMEM) supplemented with 10% fetal calf serum (FCS), IL-3 (2ng/mL), IL-6 (2ng/mL) and SCF (10ng/mL) prior to transduction. Viral supernatant was collected 48 and 72 h post transfection, mixed in a 1:1:1 ratio and spun onto RetroNectin (Takhara)-coated tissue culture plates at 2000g for 1 h. FLCs were added to the virus-coated plates and centrifuged at 500g for 4 min. Transduced FLCs were then cultured for a further 72 h prior to flow cytometry validation of transduction efficiency and transplant into murine recipients.

Transplantation and disease monitoring for the I1DN model

To generate murine leukemias, 10^6 transduced FLCs (consisting of a mixture of untransduced, single-, double- and triple-transduced cells) were transplanted into sublethally irradiated (6.5Gy administered as a single dose) *Ptprca* recipients by intravenous injection into the tail vein. For serial transplantation experiments, bone marrow or spleen cells from moribund animals were collected and cryopreserved in FCS supplemented with 10% DMSO. Cryopreserved cells were thawed and washed in Dulbecco's phosphate-buffered saline (PBS), and 1-2 x 10^5 viable cells were transplanted into sub-lethally irradiated (6.5Gy administered as a single dose) *Ptprca* recipients, or unirradiated NSG recipients, by intravenous injection into the tail vein. To reduce the occurrence of graft-vs-host disease (GvHD), I1DN cells were stained for 15 min on ice with a lymphoid lineage cocktail containing antibodies against Tcrβ (eBioscience 47-5961-82), B220 (Invitrogen 47-0452-82) and NK1.1 (BD Pharmingen 560618), then washed and resuspended in FACS buffer with DAPI. Cells were sorted on the BD FACSAria Fusion 5 for the dsR+/GFP+/DAPI-/lymphoid lineage-population before being washed, resuspended in PBS and transplanted into NSG mice.

Animals were closely monitored for clinical signs of disease development (weight loss, lethargy, hunched posture) by animal house technical staff who were blinded as to the conditions of the experiment. Peripheral blood was routinely collected by tail vein incision into EDTA coated Microvette® capillary blood collection tubes (Sarstedt AG & Co) to assess changes in blood cell counts and detect presence of leukemic cells by flow cytometry. Animals were euthanized at ethical endpoint based on clinical symptoms and overall survival rates were assessed using Kaplan-Meier analysis.

Limiting dilution transplant assay

I1DN cells were stained for 15 min on ice with antibodies against cKit (BD Pharmingen 553356), CD11b (Thermo Fisher 47-0112-82), CD34 (BD Bioscience 562608), FcγR-III (BD Optibuild 740851) and Sca1 (BD Pharmingen 558162), then washed and resuspended in FACS buffer. Cells were sorted on the BD FACSAria Fusion 5 for I1DN CMP (GFP+/CD11b-/CD117+/Sca1-/CD34^{mid}/FcγR-III^{mid}) and GMP (GFP+/CD11b-/CD117+/Sca1-/CD34^{high}/FcγR-III^{high}) cells. Sorted cells were washed and resuspended in PBS at 4 × 10^5/mL, 4 × 10^4/mL, 4 × 10^3/mL. 200 μL of cells were transplanted into NSG mice (N = 3/cell type/cell number).

I1DN therapy experiments

Mice assigned to dox treated cohorts were provided with dox supplemented chow (600 mg/kg) (Speciality Feeds) and dox water (dox 0.2% w/v, sucrose 2% w/v) for the duration of the experiment. AG-120 (150 mg/kg) was administered by twice daily oral gavage of an amorphous solid dispersion with hypromellose acetate succinate (HPMCAS) as the carrier for the active pharmaceutical ingredient. AG-120 was prepared by resuspending 3% (w/v) AG-120-SDD, 0.5% (w/v) methylcellulose and 0.2% (w/v) Tween80 in purified water. AG-120-SDD (Agios Pharmaceuticals) contained the active pharmaceutical ingredient (AG-120) in a 1:1 (w/w) ratio with HPMCAS. Vehicle was comprised of 1.5% (w/v) HPMCAS, 0.5% (w/v) methylcellulose and 0.2% (w/v) Tween80 in purified water. Vehicle and AG-120 were administered to recipient mice by oral gavage twice daily at doses relative to body weight (10 mL/kg) for the duration of the experiment defined. The treatment protocol was modified for the azacitidine and AG-120 combination study to comply with ethics requirements. Azacitidine was prepared fresh daily in PBS to a final concentration of 0.1 mg/mL and was administered by intraperitoneal injections according to body weight (1 mg/kg). Azacitidine treatment was administered once per day, in cycles of 2 days on and 1 day off, for 14 days. Mice received a 1-week treatment break, followed by another 14 days of the same azacitidine cycle. During each treatment period, AG-120 was administered once every day (150 mg/kg). On days where the combination treated group received both azacitidine and AG-120, drugs were administered at least 6 h apart.

PDX therapy experiments

AML cells #CTG-2227 collected from leukapheresis were used in this study. *IDH1*^{R132H}, *NPM1*^{W288fs*12}, *DNMT3A*^{A571fs} and *FLT3*^{ITD} mutations were detected at diagnosis. *IDH1*^{R132H} (0.56 allele frequency), *NPM1*^{W288fs*12} (0.57 allele frequency) and *DNMT3A*^{A571fs} (0.06 allele frequency) mutations were confirmed by targeted sequencing using the Trusight Myeloid sequencing panel (Illumina) prior to transplant. Within 4 h prior to inoculation, female NOG mice were sub-lethally irradiated with 1.5Gy whole body irradiation. #CTG-2227 cells were thawed at 37°C and diluted to a concentration of 10 × 10^6 cells/mL. UCHT1 antibody (BioXCell) was incubated with cells in suspension on ice for 30 min at a concentration of 1 μL/10^6 and 2 × 10^6 cells were transplanted into each recipient via injection into the lateral tail vein. Animals were treated with azacitidine at a dose level of 3mg/kg with a volume of 10mL/kg IP/Q3D, AG-120 at a dose level of 900mg/kg with a dose volume of 10mL/kg PO/QD or the combination.

AG-120 and 2-HG measurements in mouse serum

50 μL of peripheral blood was centrifuged at 2000g for 4 min at 4°C to separate the plasma from the cells. 20 μL of plasma supernatant was carefully transferred into a new eppendorf tube and immediately stored at −80°C. Bone marrow from a single femur was isolated by pulse centrifugation into an eppendorf tube and stored at −80°C. The concentrations of AG-120 in plasma and tissue samples were determined using non-validated liquid chromatography with tandem mass spectrometry (LC-MS/MS) methods. Tissue samples were homogenized using a FastPrep homogenizer for 60 s, with 10 volumes (volume-by-weight [v/w]) of methanol:water (80:20 [v/v]) to get a homogenate with a dilution factor of 11. Calibration standards and quality control (QC) samples were prepared in blank mouse plasma. A 10-μL aliquot of calibration standards, QCs, unknown plasma and tissue homogenate were mixed with 200 μL of acetonitrile containing the internal standard (IS) AGI-0018070 (25 ng/mL) for protein precipitation. The mixture was vortexed at and centrifuged. A 100-μL aliquot of supernatant was mixed with 100 μL of water with 0.1% formic acid and vortexed to mix and was analyzed on an SCIEX Triple Quad™ 6500+ with Exion LC™ AD system. A reversed-phase gradient method using a Waters ACQUITY UPLC HSS T3 Column (100Ã, 1.8μm, 2.1 mm × 50 mm) maintained at 50°C, provided chromatographic separation. Water with 0.1% formic acid and acetonitrile with 0.1% formic acid were used as mobile phase A and B respectively, at a total flow rate of 600 μL/min. AG-120 and the IS were ionized under a positive ion electrospray mode and detected through the multiple-reaction monitoring (MRM) transitions of m/z 583.2/214.0 and m/z 587.3/214.0. Data was acquired using Analyst 1.6.3 (AB Sciex, Foster City, CA). The standard curve had a coefficient of determination (R2) value > 0.98 in a linear regression with 1/X2 weighting. The quality control samples had a precision and accuracy within 20% of theoretical values. The peak area ratios of analyte relative to internal standard were used for AG-120 quantitation. Linearity was achieved in the AG-120 concentration range from 1 ng/mL to 30,000 ng/mL.

Flow cytometry analysis and cell sorting

A 10 mL single cell suspension of bone marrow in FACS buffer (2% heat inactivated FCS in PBS) from a single intact femur per mouse was obtained by mechanical dissociation, with a mortar and pestle, which was subsequently filtered through a 70 μm cell-strainer (Greiner Bio-One). One-eighth of the single cell suspension obtained from a single femur per mouse was isolated for quantitative flow cytometry. Splenocytes were isolated by pressing the spleen through a 70 μm cell-strainer with a volume of FACS buffer relative to spleen weight (1 mg/40 μL). 100 μL (equivalent to 2.5 mg spleen) of the splenocyte cell suspension was used for quantitative flow cytometry. For flow cytometric analysis and cell sorting, single-cell suspensions of whole blood, bone marrow and spleen were incubated in ACK red cell lysis buffer (150 mM NH_4Cl, 10 mM $KHCO_3$, 0.1 mM EDTA) for 2 min and then washed in FACS buffer (PBS, 2% FBS). Cells were then re-suspended in FACS buffer (2% heat inactivated FCS in PBS) and stained with fluorophore-conjugated antibodies targeted against cell surface markers. All FACS antibodies in the Key resources table were diluted 1/200, except for CD34 which was diluted 1/100 and Ly-6G which was diluted 1/400. Cells were stained for 15 min on ice or 5 min in a 37°C water bath, washed then resuspended in FACS buffer. Cells were analyzed on the BD LSR Fortessa X-20 or BD FACSymphony or sorted on the BD FACSAria Fusion 5 or BD FACSAria Fusion 3 (BD Biosciences). Data was analyzed using FlowJo (v 10.4).

Western blot

Bone marrow and spleen derived I1DN cells sorted by FACS, were pelleted by centrifugation (450 x g, 4 min, 4°C). Pelleted cells were washed with PBS and lysed for 1 h on ice in RIPA buffer (NaCl 150 mM, $MgCl_2$ 2 mM, Triton X-100 1% (v/v), Sodium Deoxycholate 0.5% (w/v), SDS 0.1% (w/v), Tris-Cl 50 mM pH 8.0) with 1 x protease inhibitor cocktail (Roche Diagnostics) and Bezonase 1.25 U/uL (Merk Millipore). Protein concentration was quantified using the Microplate Procedure with the Pierce BCA Protein Assay Kit (Thermo Scientific) according to the manufacturer's instructions and used to calculate the concentration of the samples. 20–40 μg of protein lysates were diluted to 1–2 μg/μL with PBS and 6 x SDS (Tris base 375 nM pH 6.8, SDS 12.3% (w/v), Glycerol 25.8% (v/v), bromophenol blue 600 μg/mL, 2-mercaptoethanol 60 μL/mL). Samples were incubated at 95°C for 5 min prior to being resolved on a 4–15% Mini-PROTEAN TGX Precast Protein Gels (Bio-rad) and transferred onto a methanol activated Immobilon-P PVDF membrane (Millipore) by electroblotting in transfer buffer (Tris base 25 mM, glycine 1.92 M, methanol 10% (v/v)) for 60 min at 4°C. Membranes were blocked in 5% (w/v) skim milk powder in 1 x TBS/T (Tris base 50 mM pH 7.6, NaCl 150 nM, Tween 20 0.1% (v/v)) for 1 h at room temperature prior to incubation in primary antibody (Key resources table) diluted in 5% (w/v) skim milk powder in 1 x TBS/T overnight at 4°C. Membranes were washed with 1 x TBS/T for 15 min in 5 min intervals before incubation in HRP-conjugated secondary

antibody diluted in 5% (w/v) skim milk powder in 1 x TBS/T for 1 h at room temperature. Membranes were subsequently washed with 1 x TBS/T for 30 min in 10 min intervals prior to incubation in ECL™ (GE Healthcare, cat# RPN2106) and exposure by film (FUJIFILM Super RX) using an AGFA CP1000 developer (AGFA).

RNA sequencing and analysis

1–5 × 10^5 cells ($GFP^+cKit^+CD11b^-$) per mouse were isolated by FACS, washed with PBS and pelleted by centrifugation (450 x g, 10 min, 4°C) prior to being stored at −80°C in TRIzol Reagent (Invitrogen). RNA was extracted with the Direct-zol RNA Microprep kit as per manufacturer's instructions (Zymo Research). Purified RNA was quantified using the TapeStation 2200 system (Aligent) with RNA HS screentape (Aligent) according to the manufacturer's instructions. RNA was stored at −80°C until required. The Molecular Genomics Core of the Peter MacCallum Cancer Center used the QuantSeq 3′ mRNA-seq Library Prep Kit for Illumina (Lexogen), according to the manufacturer's instructions, to generate the sequencing libraries from the purified RNA. 75 bp single end reads with a depth of 6–10 million reads per sample were generated using the Illumina NextSeq500.

Sequencing reads were demultiplexed using bcl2fastq (v 2.17.1.14), low quality (Q < 30) reads removed, and trimmed at the 5′ and-3′ ends using cutadapt (v 1.14) (Martin, 2011) to remove adapter sequences and poly-A-tail derived reads respectively. Sequencing reads were mapped to the mouse reference genome (mm10) using HISAT2 (v 2.1.0) (Kim et al., 2015) and counted using the featureCounts command of the Subread package (v 1.6.3) (Liao et al., 2014). Read normalization and differential gene expression analysis was performed in R (v 3.6.2) using R packages limma (v 3.42.2) (Ritchie et al., 2015) and EdgeR (v 3.28.1) (McCarthy et al., 2012). Log2-normalized expression values of selected pyrimidine metabolism genes from normal human hematopoietic cells (GSE42519) (Rapin et al., 2014) were downloaded from BloodSpot (https://servers.binf.ku.dk/bloodspot). Normalized expression values of normal mouse hematopoietic cells (GSE60101) (Lara-Astiaso et al., 2014) were downloaded from GEO, converted to CPM and log2-normalized. RCisTarget (v 1.11.10) (Aibar et al., 2017) was used for motif enrichment analysis. Barcodeplots (limma) were used to visualize gene set enrichment and rotating gene set testing (using the "fry" function from the limma package) was used to test for gene set enrichment. R packages pheatmap (v 1.0.12), ggplot2 (v 3.2.1), ggrepel (v 0.8.1), RColorBrewer (v 1.1–2) and limma (v 3.42.2) (Ritchie et al., 2015) were used to generate figures.

RRBS sequencing and analysis

5 × 10^4 cells ($GFP^+cKit^+CD11b^-$) per mouse were isolated by FACS, washed with PBS and pelleted by centrifugation (450 x g, 10 min, 4°C). DNA was extracted using the Quik-DNA Microprep Kit (Zymo Research) as per the manufacturer's instructions. Diagenode's Premium RRBS kit was used according to the manufacturer's instructions to generate the RRBS libraries from the purified DNA. Each sample contained methylated and unmethylated spike-in controls, as per the instructions in Diagenode's Premium RRBS kit. Libraries were sequenced on the Illumina Novaseq6000 with 150 bp paired-end reads and a depth of at least 30 million reads per sample.

Sequencing reads were demultiplexed using bcl2fastq (v 2.17.1.14), low quality reads removed, and trimmed with TrimGalore (v 0.4.4) using –paired and –rrbs settings. Bismark (v 0.22.3) (Krueger and Andrews, 2011) was used to map the spike-in controls and samples using default parameters, and samtools (v 1.4.1) (Li et al., 2009) was used to sort and index bam files. Bismark (v 0.22.3) (Krueger and Andrews, 2011) was used to extract coverage files, and differential analysis was performed in R (v 4.0.2) using the standard edgeR (v 3.32) workflow for differential methylation analysis (Chen et al., 2017). Briefly, CpGs were annotated to the closest TSS using edgeR's nearestTSS function and subset to include CpGs that lie within 2kb upstream and 1kb downstream of any given TSS, then counts were summed over each gene's TSS, promoter regions with low coverage removed (promoters retained when methylated + unmethylated counts ≥10 in every sample), and dispersion estimation and model fitting as per edgeR guidelines.

Exome sequencing and analysis

Sequencing reads were aligned using BWA-MEM (Li, 2013) using reference genome GRCm38.73, and the aligned reads were processed through three variant callers: MuTect v1.17 (Cibulskis et al., 2013), Vardict v1.4.6 (Lai et al., 2016), and GATK-Mutect2 v3.9.0 (Van der Auwera et al., 2013). Resulting variants were annotated using Variant Effect Predictor (VEP) release 90 (McLaren et al., 2016). Other utility software involved in the pipeline includes BEDTools v2.21.0 (Quinlan and Hall, 2010) for region filtering, BCFtools v1.3.1 (Danecek et al., 2021) for variant processing and filtering, and Tabix v0.2.5 (Li, 2011) for indexing. In R (v 4.0.2), variants detected in at least 2 of the variant callers were retained, low quality (QUAL <30) and low read depth variants (PMCDP <10) were excluded and variants with VAF <0.3 in the I1DN TE leukemias were excluded. Additionally, for variants that affected multiple transcripts of the same gene, the variant predicted to have the greatest impact was retained and the rest were excluded. ggplot2 (3.3.3) was used for figure generation.

Single-cell RNA sequencing and analysis

I1DN progenitor cells were FACS sorted into PBS/2%FBS. Cells were washed once with RNase free PBS/1%BSA and resuspended in PBS/1%BSA+0.2U/mL RNase inhibitor (Protector RNAse inhibitor, Sigma) at a final concentration of 1000 cells/μL. Cell suspensions were loaded onto separate channels of the 10XChromium Single Cell Chip and single cells were captured in droplet emulsions using the 10X Chromium Single-Cell Instrument. Reverse transcription, cDNA amplification and library preparation were performed

using the Chromium Single Cell 5′ Library & Gel Bead Kit (10X Genomics). Libraries were pooled and sequenced on the Illumina NovaSeq 6000 system with 150 bp paired end reads to a depth of ~50,000 reads per cell.

Count matrices were generated from demultiplexed scRNA-seq fastq files using the 10X Genomics Cell Ranger v3.1.0 count pipeline against the mm10/GRCm38 genome. scRNA-seq quality control, normalization, data integration, dimensional reduction, k-nearest neighbor graph construction and clustering were performed using Seurat (v 4.0.4) (Butler et al., 2018) in R (v 4.0.2). Low quality cells were removed by filtering out cells that had fewer than 1000 genes, fewer than 2000 unique molecular identifiers (UMIs), or greater than 15% mitochondrial RNA content. Seurat's CellCycleScoring function was used to assign cell cycle phase using Seurat's inbuilt list of cell cycle genes (Butler et al., 2018; Tirosh et al., 2016). Seurat's SCTransform function was used for data normalization with percentage mitochondrial reads, and differences in cell cycle phase amongst proliferating cells (S and G2M cell cycle phase scores) included in the regression model as sources of technical variation to remove. Datasets were integrated using canonical correlation analysis (CCA) within Seurat using default parameters. The first 40 principal components were used to compute a non-linear dimensional reduction using the Uniform Manifold Approximation and Projection (UMAP) method, and clustering was performed at a resolution of 0.4. Clusters with fewer than 100 cells were combined with larger clusters based on correlation analysis of the cluster-average expression of the top 500 most variably expressed genes. Pseudo-bulk RNAseq was performed for differential gene expression analysis between treatment conditions. Counts were summed across I1DN progenitor groups for each treatment condition. Differential gene expression within each I1DN progenitor group was performed with edgeR (v 3.32.1) (McCarthy et al., 2012). Gene ontology and GSEA analyses were performed with R packages clusterProfiler (v 3.18.0) (Yu et al., 2012), and fgsea (v 1.16.0) (Korotkevich et al., 2021), respectively. Seurat, ggplot2 (3.3.3) and pheatmap (1.0.12) were used for figure generation.

QUANTIFICATION AND STATISTICAL ANALYSIS

Statistical analyses were performed with R or GraphPad Prism (v9) software using statistical tests indicated in the text and figure legends.